PHYSICAL REVIEW D **71,** 083002 (2005)

Diagnostic potential of cosmic-neutrino absorption spectroscopy

Gabriela Barenboim*

Departament de Física Teòrica, Universitat de València, Carrer Dr. Moliner 50, E-46100 Burjassot (València), Spain

Olga Mena Requejo† and Chris Quigg‡

Theoretical Physics Department, Fermi National Accelerator Laboratory, P.O. Box 500, Batavia, Illinois 60510, USA

(Received 14 December 2004; published 5 April 2005)

Annihilation of extremely energetic cosmic neutrinos on the relic-neutrino background can give rise to absorption lines at energies corresponding to formation of the electroweak gauge boson Z^0. The positions of the absorption dips are set by the masses of the relic neutrinos. Suitably intense sources of extremely energetic (10^{21}–10^{25}-eV) cosmic neutrinos might therefore enable the determination of the absolute neutrino masses and the flavor composition of the mass eigenstates. Several factors—other than neutrino mass and composition—distort the absorption lines, however. We analyze the influence of the time evolution of the relic-neutrino density and the consequences of neutrino decay. We consider the sensitivity of the line shape to the age and character of extremely energetic neutrino sources, and to the thermal history of the Universe, reflected in the expansion rate. We take into account Fermi motion arising from the thermal distribution of the relic-neutrino gas. We also note the implications of Dirac vs. Majorana relics, and briefly consider unconventional neutrino histories. We ask what kinds of external information would enhance the potential of cosmic-neutrino absorption spectroscopy, and estimate the sensitivity required to make the technique a reality.

DOI: 10.1103/PhysRevD.71.083002 PACS numbers: 96.40.Tv, 13.35.Hb, 14.60.Pq, 95.35.+d

I. INTRODUCTION

A. A brief history of relic neutrinos

According to the standard cosmology, neutrinos should be the most abundant particles in the Universe, after the photons of the cosmic microwave background (CMB), provided that they are stable over cosmological times.[1] Because they interact only weakly, neutrinos decoupled when the age of the Universe was ≈ 0.1 s and the temperature of the Universe was a few MeV. Accordingly, relic neutrinos have been present—as witnesses or participants—for landmark events in the history of the Universe: the era of big-bang nucleosynthesis, a few minutes into the life of the Universe; the decoupling era around 379 000 yrs [8], when the cosmic microwave background was imprinted on the surface of last scattering; and the era of large-scale structure formation, when the Universe was only a few percent of its current age.[2]

Some of the earliest cosmological bounds on neutrino masses followed from the requirement that massive relic neutrinos, present today in the expected numbers, do not saturate the critical density of the Universe [10,11]. Refined analyses, incorporating constraints from a suite of cosmological measurements, sharpen the bounds on the sum of light-neutrino masses [12]. The discovery of neutrino oscillations [13–15] implies that neutrinos have mass, but we cannot reliably compute the contribution of relic neutrinos to the dark matter of the Universe until we establish the absolute scale of neutrino masses. Current estimates for the neutrino fraction of the Universe's mass-energy density lie in the range $0.1\% \lesssim \Omega_\nu \lesssim 1.5\%$.

The neutrino gas that we believe permeates the present Universe has never been detected directly. Imaginative schemes have been proposed to record the elastic scattering of the 1.95-K relic neutrinos, but all appear to require significant further technological development before they can approach the needed sensitivity [16,17]. In this paper, we elaborate a complementary approach: detecting relic neutrinos by observing the resonant annihilation of extremely high-energy cosmic neutrinos on the background neutrinos through the reaction $\nu\bar{\nu} \to Z^0$ [18–23]. By observing Z bursts or absorption lines, one may hope to determine the absolute neutrino masses and the flavor composition of the neutrino mass eigenstates.[3]

As a *Gedankenexperiment,* the prospect of cosmic-neutrino absorption spectroscopy has great clarity and appeal. Reality is more complicated, and it is our purpose—building on earlier work—to analyze all the important effects that will influence the execution and interpretation of neutrino-absorption experiments. We are encouraged in this effort by the imminent construction and operation of neutrino observatories and by imaginative

*Electronic address: Gabriela.Barenboim@uv.es
†Electronic address: omena@fnal.gov
‡Electronic address: quigg@fnal.gov

[1]For compact summaries of the canonical thermal history of the Universe, see Weinberg [1], Sec. 15.6, the review article by Steigman [2], Secs. 19–23 of the *Review of Particle Physics* [3], or a standard textbook [4–7].

[2]For a recent quantitative assessment of evidence that neutrinos were present at these times, see Ref. [9].

[3]See Ref. [24] for a general review of other aspects of particle physics at neutrino observatories.

efforts to develop new techniques to detect superhigh-energy neutrinos. A novel aspect of the analysis presented here is our attention to the thermal motion of the relics. We also raise the possibility that cosmic-neutrino absorption spectroscopy might open a new vista on the thermal history of the Universe, as well as extending or validating our understanding of neutrino properties.

In the body of this introductory section, we develop the pieces that enter the analysis of neutrino absorption spectra: our expectations for the relic-neutrino background now and in the past, details of the annihilation cross section, and possible sources of extremely energetic cosmic neutrinos. We also survey experiments that aim to detect ultrahigh-energy neutrinos. In Sec. II, we describe the idealized situation of a superhigh-energy neutrino beam incident on a (very long) uniform column of relic neutrinos at today's density, but with negligible temperature. We describe the information that could be extracted from absorption dips, assuming perfect energy resolution and flavor tagging.

The extremely long interaction length for neutrinos traversing the relic background means that we must integrate over cosmic time, or redshift, and this takes up Sec. III. There we discuss the mechanisms that distort absorption lines and how the distortions compromise the dream of determining the absolute neutrino masses. We also remark on the sensitivity of the line shape to the thermal history of the Universe.

We include Fermi motion due to the relic-neutrino temperature—which evolves with redshift—in Sec. IV. The mean relic-neutrino momentum at the present epoch acts as a rough lower bound on the effective target mass. Section V is devoted to the implications of unconventional neutrino histories, including neutrino decay and the consequences of a lepton asymmetry in the early Universe. We summarize what we have learned, and assess the prospects for experimental realization of these ideas in Sec. VI. Looking forward to the experiments, we consider how external information could enhance the potential of cosmic-neutrino absorption spectroscopy, and we estimate the sensitivity required to make the technique a reality.

B. Character of the relic-neutrino background

The cosmic microwave background is characterized by a Bose-Einstein blackbody distribution of photons (per unit volume)[4]

$$\frac{dn_\gamma(T)}{d^3p} = \frac{1}{(2\pi)^3}\frac{1}{\exp(p/T)-1}, \tag{1}$$

where p is the relic momentum and T is the temperature of the photon ensemble. The number density of photons throughout the Universe is

$$n_\gamma(T) = \frac{1}{(2\pi)^3}\int d^3p\,\frac{1}{\exp(p/T)-1} = \frac{2\zeta(3)}{\pi^2}T^3, \tag{2}$$

where $\zeta(3)\approx 1.20205$ is Riemann's zeta function. In the present Universe, with a photon temperature $T_0 = (2.725\pm 0.002)$ K [8], the photon density is

$$n_{\gamma 0} \equiv n_\gamma(T_0) \approx 410\ \mathrm{cm}^{-3}. \tag{3}$$

The present photon density provides a reference for other big-bang relics. The essential observation is that neutrinos decoupled when the cosmic soup cooled to around 1 MeV, so did not share in the energy released when electrons and positrons annihilated at $T\approx m_e$, the electron mass. Applying entropy conservation and counting interacting degrees of freedom, it follows that the ratio of neutrino and photon temperatures (below m_e) is

$$T_\nu/T = (\tfrac{4}{11})^{1/3}, \tag{4}$$

so that the present neutrino temperature is

$$T_{\nu 0} = (\tfrac{4}{11})^{1/3}T_0 = 1.945\ \mathrm{K} \longrightarrow 1.697\times 10^{-4}\ \mathrm{eV}. \tag{5}$$

The momentum distribution of relic neutrinos follows the Fermi-Dirac distribution (with zero chemical potential),

$$\frac{dn_{\nu_i}(T_\nu)}{d^3p} = \frac{dn_{\nu_i^c}(T_\nu)}{d^3p} = \frac{1}{(2\pi)^3}\frac{1}{\exp(p/T_\nu)+1}. \tag{6}$$

The number distribution of relic neutrinos is therefore

$$n_{\nu_i}(T_\nu) = n_{\nu_i^c}(T_\nu) = \frac{1}{(2\pi)^3}\int d^3p\,\frac{1}{\exp(p/T_\nu)+1} = \frac{3\zeta(3)}{4\pi^2}T_\nu^3 = \frac{3}{22}n_\gamma(T). \tag{7}$$

In the present Universe, the number density of each (active) neutrino species is[5]

$$n_{\nu_i 0} = n_{\nu_i^c 0} \equiv n_{\nu_i}(T_{\nu 0}) \approx 56\ \mathrm{cm}^{-3}, \tag{8}$$

and the mean momentum of relic neutrinos today is

$$\langle p_{\nu 0}\rangle = \frac{7}{2}\frac{\zeta(4)}{\zeta(3)}\cdot T_{\nu 0} \approx 3.151 T_{\nu 0} \approx 5.314\times 10^{-4}\ \mathrm{eV}, \tag{9}$$

where we have used $\zeta(4) = \pi^4/90 = 1.08232$. In the same way, the mean-squared neutrino momentum is given by

$$\langle p_{\nu 0}^2\rangle = 15\frac{\zeta(5)}{\zeta(3)}\cdot T_{\nu 0}^2 \approx 12.94 T_{\nu 0}^2, \tag{10}$$

[4]We adopt units such that $\hbar = 1 = c$, and we will measure temperature in kelvins or electron volts, as appropriate to the situation. The conversion factor is Boltzmann's constant, $k = 8.617\,343\times 10^{-5}\ \mathrm{eV\,K}^{-1}$.

[5]The unconventional neutrino histories described in Sec. V can alter this expectation.

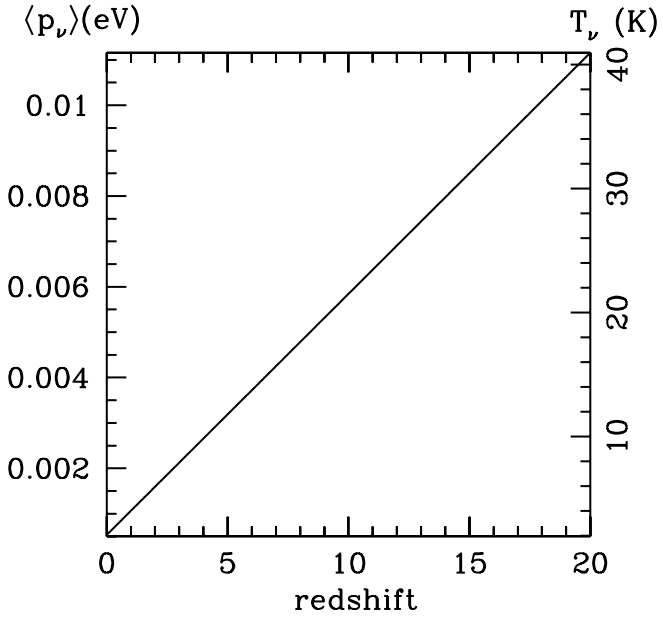

FIG. 1. Neutrino temperature T_ν (right-hand scale) and mean momentum p_ν of relic neutrinos (left-hand scale) as a function of the redshift z.

so that

$$\langle p_{\nu 0}^2 \rangle^{1/2} \approx 3.597 T_{\nu 0} \approx 6.044 \times 10^{-4}\ \text{eV}. \tag{11}$$

Neutrinos decoupled very early in the history of the Universe, at redshift $z = \mathcal{O}(10^{10})$. The temperature of a massless decoupled species scales as $T \sim (1+z)$, as shown in Fig. 1 for redshifts since the formation of the first stars [8]. By Eq. (7), this means that the relic-neutrino number densities will be redshifted as $n_{\nu_i}(z) = n_{\nu 0}(1+z)^3$. The dependence of the relic-neutrino number on the redshift is depicted in Fig. 2.

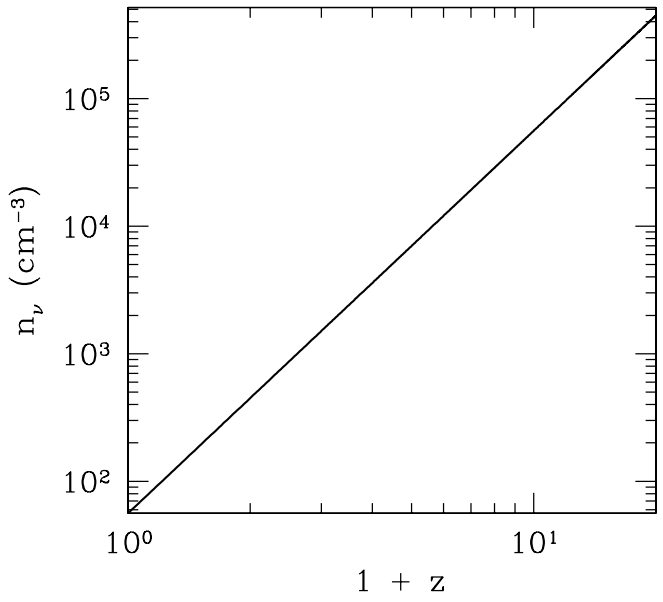

FIG. 2. Relic-neutrino number density versus redshift.

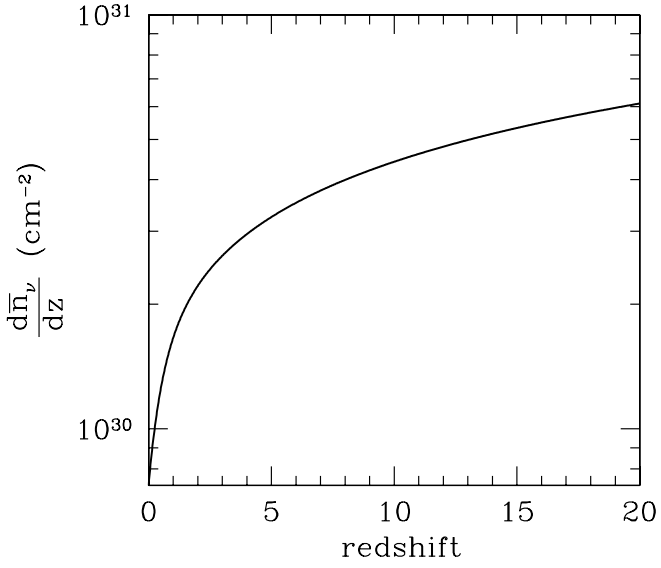

FIG. 3. Column density (14) versus redshift for the ΛCDM model, with $\Omega_m = 0.27 \pm 0.04$, $\Omega_\Lambda = 0.73 \pm 0.04$, and $h = 0.71^{+0.04}_{-0.03}$ [3].

The effective relic-neutrino density that an extremely high-energy neutrino would encounter while traversing the expanding Universe is the neutrino density per unit redshift. The propagation distance r is related to the redshift z through

$$dr = dz/(1+z)H(z), \tag{12}$$

where $H(z)$ is the Hubble parameter. In a flat Universe with negligible radiation component, we may write

$$H^2(z) = H_0^2[\Omega_m(1+z)^3 + \Omega_\Lambda], \tag{13}$$

where Ω_m is the matter density, Ω_Λ is the cosmological constant, and $H_0 = h \cdot 100\ \text{km/s Mpc}^{-1}$ is the present value of the Hubble constant. The neutrino density per unit redshift, sometimes called the *column density*, is then

$$\bar{n}_{\nu_i}(z) = n_{\nu 0}(1+z)^3 dr = \frac{n_{\nu 0}(1+z)^3 dz}{(1+z)H(z)} = \frac{n_{\nu 0}(1+z)^2 dz}{H(z)}. \tag{14}$$

In Fig. 3 we show this column density as a function of the redshift for the ΛCDM model,[6] that is, a flat Universe with a cosmological constant and cold dark matter.

The appearance of the Hubble parameter in Eq. (14) raises the possibility that careful observation of neutrino absorption lines could reveal something of the thermal

[6]For three complementary views of today's concordance cosmology, see Refs. [25–27].

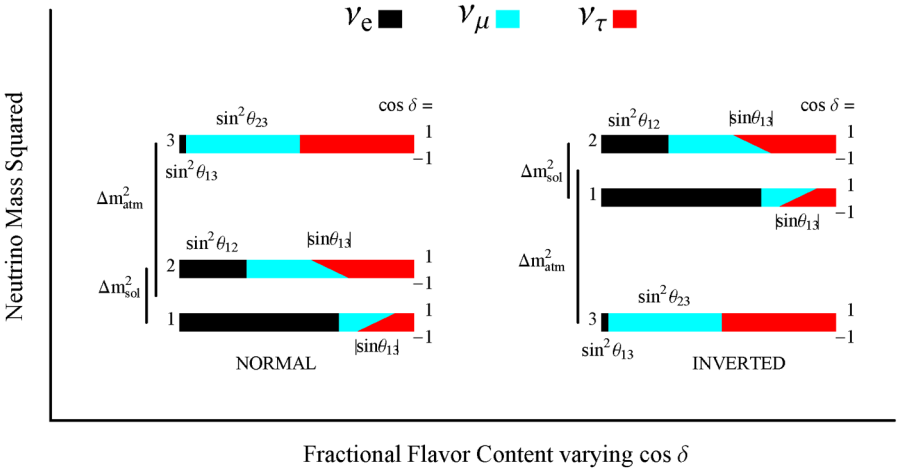

FIG. 4 (color online). Composition of the neutrino mass eigenstates (ν_1, ν_2, ν_3) in terms of the flavor eigenstates (ν_e, ν_μ, ν_τ) for the normal (left panel) and inverted (right panel) hierarchies (from Ref. [132]). Each bar shows the flavor mixture of a mass eigenstate as the CP-violating phase, δ, varies from $\cos\delta = -1$ (bottom) to $\cos\delta = 1$ (top). The other mixing parameters are held fixed at the representative values $\sin^2\theta_{12} = 0.30$, $\sin^2\theta_{13} = 0.03$ and $\sin^2\theta_{23} = 0.50$. To an excellent approximation, $\Delta m^2_{12} = \Delta m^2_{\rm sol}$ and $\Delta m^2_{23} = \Delta m^2_{\rm atm}$.

history of the Universe. We shall see in Sec. III examples of how the line shapes differ in different cosmologies.

C. The neutrino mass spectrum

Through the past few years, experiments have adduced robust evidence for flavor change involving solar, atmospheric, and reactor neutrinos, as well as neutrinos produced by accelerator beams [28]. Putting aside exotic interpretations, these results establish that neutrinos have nonvanishing masses and that neutrino species mix. The most economical description of the new phenomena is given in terms of the 3×3 neutrino-mixing matrix that relates flavor eigenstates to mass eigenstates,[7] the analogue of the (Cabibbo-Kobayashi-Maskawa) quark mixing matrix. The standard neutrino-mixing phenomenology entails six parameters: three real mixing angles (θ_{12}, θ_{23}, θ_{13}), one Dirac CP phase (δ), and two independent mass-squared differences[8] (Δm^2_{12} and Δm^2_{23}).

To connect the solar, atmospheric, reactor, and accelerator observations with neutrino parameters, we follow convention [31] in identifying the mass splittings and mixing angles that drive the solar and atmospheric transitions as (Δm^2_{12}, θ_{12}) and ($|\Delta m^2_{23}|$, θ_{23}). The sign of the mass splitting between the atmospheric state ν_3 and the solar doublet (ν_1, ν_2) is not yet known. Both the normal hierarchy ($m_3 > m_2 > m_1$) and the inverted hierarchy ($m_3 < m_1 \lesssim m_2$) are illustrated in Fig. 4, where the colored (shaded) bars represent the flavor content of the mass eigenstates.

The best-fit point for the combined analysis of solar neutrino data together with KamLAND reactor data [32] is at $\Delta m^2_{12} = 8.2^{+0.6}_{-0.5} \times 10^{-5}$ eV^2 and $\tan^2\theta_{12} = 0.40^{+0.09}_{-0.07}$. In the atmospheric neutrino sector, the most recent analysis of K2K (KEK-to-Kamioka) accelerator data and atmospheric neutrino data constrains 1.9×10^{-3} eV$^2 < |\Delta m^2_{23}| < 3.0 \times 10^{-3}$ eV^2, $\sin^2 2\theta_{23} > 0.90$ [33,34].

Only an upper bound exists on the mixing angle θ_{13} (which connects the solar and atmospheric neutrino realms), and the CP-violating phase δ is unobservable in current neutrino-oscillation experiments, so we allow in Fig. 4 for the variation $-1 < \cos\delta < +1$. The CHOOZ reactor experiment bounds $\sin^2 2\theta_{13} < 0.1$ (at 90% C.L.) for a value of the atmospheric mass gap close to the current central value [35].

Several oscillation experiments that exploit neutrino beams from nuclear reactors and accelerators are taking data, and similar experiments will take data over the next few years. In particular, future reactor neutrino experiments could set the value of θ_{13}, as explored in detail in Ref. [36]. For a recent study of the measurement of leptonic CP violation and the pattern of the neutrino mass spectrum at the future T2K (Tokai-to-Kamioka) [37] and NOvA [38] long-baseline experiments, see Ref. [39]. If the value of θ_{13} turns out to be very small, the ultimate high-precision measurements may require superbeams [40], neutrino factories [41,42], beta beams [43], or a combination [44,45].

Despite the great promise of planned and future neutrino-oscillation experiments, two essential neutrino properties would still remain unknown. Is the neutrino

[7]We consider here the canonical picture of three neutrino families. The ongoing Mini-BooNE experiment [29] is expected to explore all the parameter space of the $\nu_\mu \leftrightarrow \nu_e$ mutation claimed by the LSND experiment [30], with its implication of additional (presumably sterile) neutrinos. The neutrino-mixing matrix is sometimes called the Pontecorvo-Maki-Nakagawa-Sakata matrix.

[8]We define $\Delta m^2_{ij} \equiv m^2_j - m^2_i$, where m_i is the mass of ν_i.

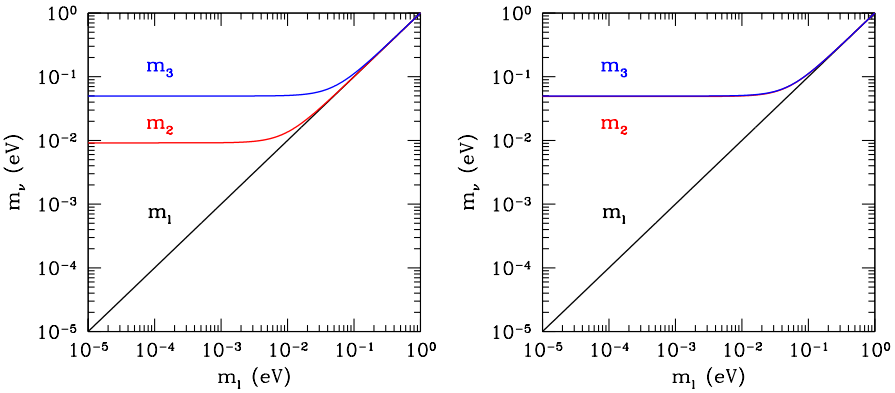

FIG. 5 (color online). Favored values for the neutrino masses as functions of the lightest neutrino mass, m_ℓ, in the three neutrino scenario for normal hierarchy (left panel, $m_\ell = m_1$) and the inverted hierarchy (right panel, $m_\ell = m_3$). (After Ref. [133].)

distinct from its antiparticle ($\nu \neq \bar{\nu}$, Dirac case), or identical to it ($\nu \equiv \bar{\nu}$, Majorana case)?[9] What are the absolute values of the neutrino masses?

Searches for neutrinoless double beta decay, a rare—and hitherto unobserved—transition between two nuclei with the same mass number (A) that changes the nuclear charge (Z) by two units,

$$(Z, A) \rightarrow (Z + 2, A) + e_1^- + e_2^-, \tag{15}$$

are for now our only probe for Majorana neutrinos. Observational upper limits on $\beta\beta(0\nu)$ rates provide an upper bound on the so-called *"effective Majorana mass"* of the electron neutrino [3],

$$\langle m_{\rm eff} \rangle < 0.3\text{–}1.0 \text{ eV}. \tag{16}$$

Forthcoming $\beta\beta(0\nu)$ experiments that aim for sensitivity approaching $\langle m_{\rm eff} \rangle \lesssim 0.05$ eV could well establish neutrinos as Majorana particles [50,51].

Direct information on the absolute scale of neutrino masses can be extracted from kinematical studies. The present upper bound on the electron-neutrino mass from tritium beta-decay experiments is 2.2 eV (95% C.L.) [52,53], and in the future the KATRIN experiment is expected to be sensitive to electron-neutrino masses approaching 0.2 eV (90% C.L.) [54].

The evolution of the Universe is sensitive to the absolute neutrino mass scale, independent of mixing parameters or CP-violating phases [55,56], for example, through the influence of neutrinos on the matter power spectrum [57,58]. Combining Wilkinson Microwave Anisotropy Probe observations of the cosmic microwave background with large-scale structure data from the 2dF Galaxy Redshift Survey [59] or the Sloan Digital Sky Survey [60] yields impressive constraints on neutrino mass $\sum_i m_{\nu_i} \lesssim 1$ eV, the precise value depending on the priors and the data set [12,61]. However, the neutrino mass limits arising from existing large-scale structure can be evaded if new interactions (such as the coupling of neutrinos to a light boson) enable the relic neutrinos to annihilate at late times [62].

In Fig. 5 we show the allowed ranges of neutrino masses (m_1, m_2, m_3) in terms of the lightest neutrino mass m_ℓ for the normal and inverted hierarchies, using the best-fit values of the solar and atmospheric mass gaps reported above. For the entire range of permitted masses, at least two relic species are nonrelativistic ($m_\nu \gg \langle p_{\nu 0} \rangle$) in the present Universe. Consult Refs. [63,64] for recent surveys of the prospects for determining the absolute mass scale of the neutrinos.

D. The absorption cross section

In terrestrial experiments that seek to detect neutrinos originating in particle accelerators or astrophysical sources, the reactions of interest are usually the deeply inelastic scattering processes $\nu N \rightarrow \mu +$ anything or $\nu N \rightarrow \nu +$ anything. Nucleons are so rare throughout the Universe at large [$n_B = (2.5 \pm 0.1) \times 10^{-7}$ cm^{-3} in the current Universe [3]] that neutrino-nucleon scattering is a negligible source of attenuation, even over cosmological distances. A path length of 8×10^5 Mpc in today's Universe corresponds to 1 cm water equivalent (cmwe).

It is convenient to define the interaction length,

$$\mathcal{L}_{\rm int}^{\nu N} = 1/\sigma_{\nu N}(E_\nu) N_A, \tag{17}$$

where $\sigma_{\nu N}$ is the appropriate neutrino-nucleon cross section and $N_A = 6.022 \times 10^{23}$ mol^{-1} $= 6.022 \times 10^{23}$ cm^{-3} (water equivalent) is Avogadro's number. For neutrino energies in the range 10^{16} eV $\lesssim E_\nu \lesssim 10^{21}$ eV, a recent

[9] Prevailing theoretical opinion favors the Majorana character, if only because we know no principle that forbids Majorana mass terms. The seesaw mechanism [46–48] offers a natural interpretation of the smallness of neutrino masses, and points to a new scale associated with the heavy Majorana neutrino. The seesaw mechanism implies lepton-number–violating processes that could have happened in the early Universe. The decay of the heavy, weak-isoscalar, Majorana neutrinos, together with $B + L$-violating sphaleron transitions can give rise to the baryon asymmetry of the Universe [49].

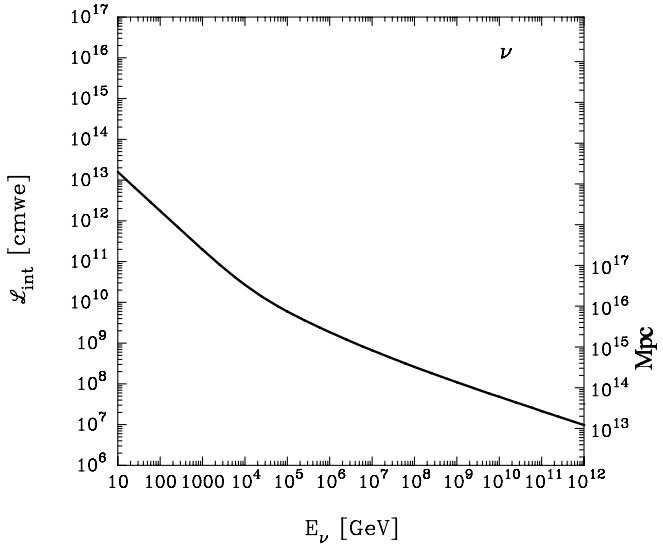

FIG. 6. Interaction length defined in Eq. (17) for the reactions $\nu N \to$ anything as a function of the incident-neutrino energy. The left-hand scale, in cmwe, is appropriate for terrestrial applications; the right-hand scale, in Mpc for the current Universe, is appropriate for transport over cosmological distances. (After Ref. [65].)

calculation [65] yields $(\nu, \bar{\nu})N$ total cross sections

$$\sigma_{\nu N\to \rm all} \approx 0.78 \times 10^{-35}\ {\rm cm}^2 \left(\frac{E_\nu}{1\ {\rm GeV}}\right)^{0.363}. \qquad (18)$$

It is not unreasonable to extrapolate this form a few orders of magnitude higher in energy.[10]

We plot the resulting interaction length in Fig. 6. For the energies that will be of interest to us, the interaction length lies in the range 10^6–10^9 cmwe, or 10^{12}–10^{15} Mpc in the current Universe. These distances are extraordinarily vast, in view of the expectation that astrophysical sources of ultrahigh-energy neutrinos such as active galactic nuclei lie within 100 Mpc of Earth. At earlier—but not too early—epochs, the nucleon density scales with redshift as $n_B(z) = n_B(0)(1+z)^3$. Even so, back to $z \approx 20$ when the first astrophysical neutrino sources began to shine, the interaction length is far too long for νN scattering to be a significant mechanism for reducing the flux of neutrinos incident on Earth.[11]

Over the energy range of interest for neutrino astronomy, the interactions of $\nu_e, \nu_\mu, \nu_\tau, \bar{\nu}_\mu, \bar{\nu}_\tau$ with electrons can generally be neglected compared to interactions with nucleons. The case of $\bar{\nu}_e e$ interactions is exceptional, because of the intermediate-boson resonance formed in the neighborhood of $E_\nu^{W\rm res} = M_W^2/2m_e \approx 6.3 \times 10^{15}$ eV. The peak cross section, $\sigma(\bar{\nu}_e e \to W^- \to \text{anything}) \approx 5 \times 10^{-31}$ cm^2, corresponds to an interaction length at resonance of 6×10^6 cmwe [67]. Assuming that the density of electrons throughout the current Universe is comparable to the density of baryons, even resonant $\bar{\nu}_e e$ scattering contributes a negligible attenuation of astrophysical neutrinos *en route* to Earth.

The number density of relic neutrinos (of each species) in the current Universe is some 220×10^6 times the number density of baryons. The thicker relic-neutrino target combined with an appreciable cross section for $\nu\bar{\nu} \to Z^0$ annihilation accounts for the importance of resonant absorption as an attenuator of extremely high-energy neutrinos. As we will see shortly, the interaction length for resonant annihilation in the current Universe is $\mathcal{L}_{\rm int}^{\nu\bar{\nu}} \approx 1.2 \times 10^4$ Mpc, some 6 orders of magnitude shorter than the interaction lengths for νN or resonant $\bar{\nu}_e e$ scattering.

The cross section for neutrino-antineutrino annihilation into fermion pairs through the Z^0 is given by

$$\sigma^{s:Z}(\nu_\alpha \bar{\nu}_\alpha \to f\bar{f}) = \frac{G_F^2 m_i E_\nu N_c^{(f)}}{3\pi} \frac{L_f^2 + R_f^2}{(1-\mathcal{Y})^2 + \Gamma_Z^2/M_Z^2}, \qquad (19)$$

where $\mathcal{Y} = 2m_i E_\nu / M_Z^2$, $G_F = 1.16637 \times 10^{-5}$ GeV^{-2} is the Fermi constant, m_i is the mass of the target (relic) neutrino, E_ν is the incident-neutrino energy, and $N_c^{(f)}$ is the number of colors of the fermion f: 1 for leptons and 3 for quarks. The chiral couplings of f are $L_f = \tau_3^{(f)} - 2Q_f \sin^2\theta_W$ and $R_f = -2Q_f \sin^2\theta_W$, where Q_f is the fermion's electric charge and $\tau_3^{(f)} = \pm 1$ is the third component of its (left-handed) weak isospin.[12]

We have written Eq. (19) for the annihilation of a neutrino of flavor α on its antineutrino counterpart. In our application, the cross section must be weighted by the probability for the mass eigenstate ν_i to contain the flavor component ν_α, which is to say, by the absolute square of the appropriate neutrino-mixing matrix element. We have also assumed that the neutrinos are Majorana particles; the difference between Majorana and Dirac particles is explained in the following Sec. I E.

When summed over the kinematically accessible decay products of Z^0, namely, the charged leptons e, μ, τ, the neutrinos ν_e, ν_μ, ν_τ, and the quarks u, d, s, c, b, (19) leads to the branching fractions collected in Table I. In our study of absorption lines, we shall regard the 20% of $Z^0 \to \nu\bar{\nu}$ decays as removed from the incident beam. In a detailed study of particular experimental circumstances, one might choose to improve this approximation.

Depending on the incident beam and the relic target, other processes may contribute. A complete catalog was given by Roulet [20], whose notation we emulate here. We

[10] For an examination of different extrapolations in energy and of the influence of exotic mechanisms, see Ref. [66].

[11] A complete treatment, taking into account redshifting of the neutrino energy, does not change the conclusions [21].

[12] We take $M_Z = 91.1876$ GeV, $\Gamma_Z = 2.4952$ GeV, $\sin^2\theta_W = 0.231$; we have taken account of fermion masses in our numerical studies.

TABLE I. Decay modes and branching fractions of the Z^0 [3].

Decay mode	Branching fraction
Hadrons ($u\bar{u} + d\bar{d} + s\bar{s} + c\bar{c} + b\bar{b}$)	70%
Charged leptons ($e^+e^- + \mu^+\mu^- + \tau^+\tau^-$)	10%
Invisible ($\nu_e\bar{\nu}_e + \nu_\mu\bar{\nu}_\mu + \nu_\tau\bar{\nu}_\tau$)	20%

present the components of the neutrino-(anti)neutrino cross sections in Fig. 7. Neutrino-antineutrino scattering in general receives a contribution from t-channel Z exchange,

$$\sigma^{t:Z}(\nu_\alpha\bar{\nu}_\beta \to \nu_\alpha\bar{\nu}_\beta) = \frac{G_F^2 m_i E_\nu}{\pi} F_1(\mathcal{Y}), \qquad (20)$$

where $F_1(\mathcal{Y}) = [\mathcal{Y}^2 + 2\mathcal{Y} - 2(1+\mathcal{Y})\ln(1+\mathcal{Y})]/\mathcal{Y}^3$. The s-t interference term is

$$\sigma^{st:Z}(\nu_\alpha\bar{\nu}_\beta \to \nu_\alpha\bar{\nu}_\beta) = \delta_{\alpha\beta}\frac{G_F^2 m_i E_\nu}{2\pi} F_2(\mathcal{Y})\frac{(\mathcal{Y}-1)}{(1-\mathcal{Y})^2 + \Gamma_Z^2/M_Z^2}, \qquad (21)$$

where $F_2(\mathcal{Y}) = [3\mathcal{Y}^2 + 2\mathcal{Y} - 2(1+\mathcal{Y})^2\ln(1+\mathcal{Y})]/\mathcal{Y}^3$.

Neutrino-antineutrino scattering to a pair of charged leptons may proceed by W exchange in the t channel,

$$\sigma^{t:W}(\nu_\alpha\bar{\nu}_\beta \to \ell_\alpha\bar{\ell}_\beta) = \frac{4G_F^2 m_i E_\nu}{\pi} F_1(\mathcal{Y}). \qquad (22)$$

For charged-lepton pair production, the interference between the s-channel Z exchange and the t-channel W exchange is

$$\sigma^{WZ}(\nu_\alpha\bar{\nu}_\beta \to \ell_\alpha\bar{\ell}_\beta) = \delta_{\alpha\beta}\frac{4G_F^2 m_i E_\nu}{\pi} F_2(\mathcal{Y})\left(\sin^2\theta_W - \frac{1}{2}\right) \times \frac{(\mathcal{Y}-1)}{(1-\mathcal{Y})^2 + \Gamma_Z^2/M_Z^2}. \qquad (23)$$

Neutrino-neutrino (or antineutrino-neutrino) elastic scattering is mediated by t-channel Z exchange, with a cross section

$$\sigma^{t:Z}(\nu_\alpha\nu_\beta \to \nu_\alpha\nu_\beta) = \frac{G_F^2 m_i E_\nu}{\pi}\frac{1}{1+\mathcal{Y}}, \qquad (24)$$

that is accompanied, for identical species, by the u-channel contribution

$$\sigma^{u:Z}(\nu_\alpha\nu_\beta \to \nu_\alpha\nu_\beta) = \delta_{\alpha\beta}\frac{G_F^2 m_i E_\nu}{\pi} \times \left[\frac{1}{1+\mathcal{Y}} + \frac{\ln(1+\mathcal{Y})}{\mathcal{Y}(1+\frac{1}{2}\mathcal{Y})}\right]. \qquad (25)$$

Above the thresholds for W^+W^- and Z^0Z^0 pair production, we include the $\nu\bar{\nu} \to$ vector-boson-pair cross sections in our numerical analysis. The effect of these processes on neutrino attenuation is minor; the relevant formulas may be found in Ref. [20].

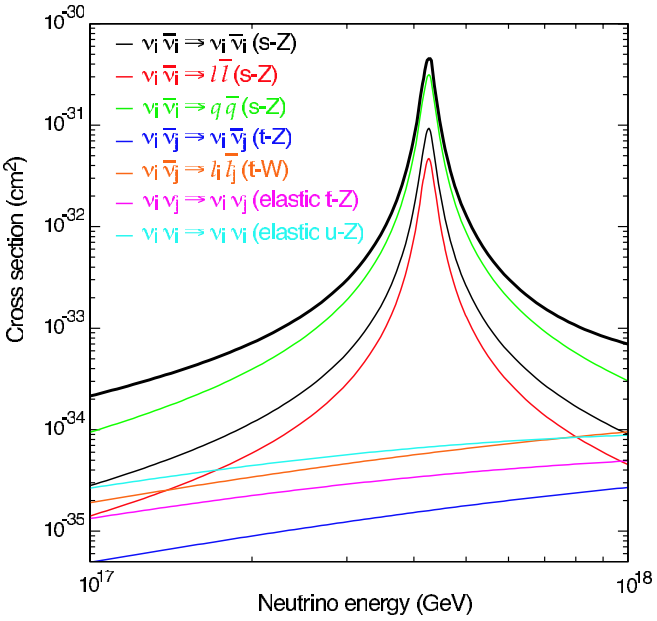

FIG. 7 (color online). Total neutrino annihilation cross section and the different contribution channels as a function of the ultrahigh neutrino energy assuming a relic-neutrino mass of $m_\nu = 10^{-5}$ eV and zero redshift.

E. Dirac versus Majorana relics

The interaction cross section may depend on whether the relic (target) neutrinos are Dirac or Majorana particles. If the relic neutrinos are extremely relativistic, the Dirac and Majorana characters are indistinguishable: relativistic neutrinos are pure left-handed chirality states, because only such states are produced in the weak interactions. Chirality and helicity coincide, and the right-handed chirality is absent. Nonrelativistic Dirac and Majorana neutrinos exhibit distinctive behavior. In the static limit, Dirac neutrinos are left-handed helicity eigenstates with equal populations of left- and right-handed chiralities; Dirac antineutrinos are right-handed helicity eigenstates, also with equal populations of left- and right-handed chiralities. Since only the left-handed neutrino (right-handed antineutrino) chiralities interact, the other two components of the Dirac-neutrino field are sterile. Because Majorana neutrinos are their own antiparticles, both chiralities interact. Accordingly, in the static limit, the interaction cross section on a Majorana target is twice the cross section on a Dirac target.

The interactions with a Majorana neutrino's "wrong-chirality" population enter with weight $m_\nu^2/(\varepsilon_\nu + p_\nu)^2$, where p_ν is the relic-neutrino momentum and $\varepsilon_\nu = \sqrt{p_\nu^2 + m_\nu^2}$, so that

$$\frac{\sigma_{\rm Majorana}}{\sigma_{\rm Dirac}} = 1 + \frac{m_\nu^2}{(\varepsilon_\nu + p_\nu)^2} = \frac{2}{1 + p_\nu/\varepsilon_\nu}. \qquad (26)$$

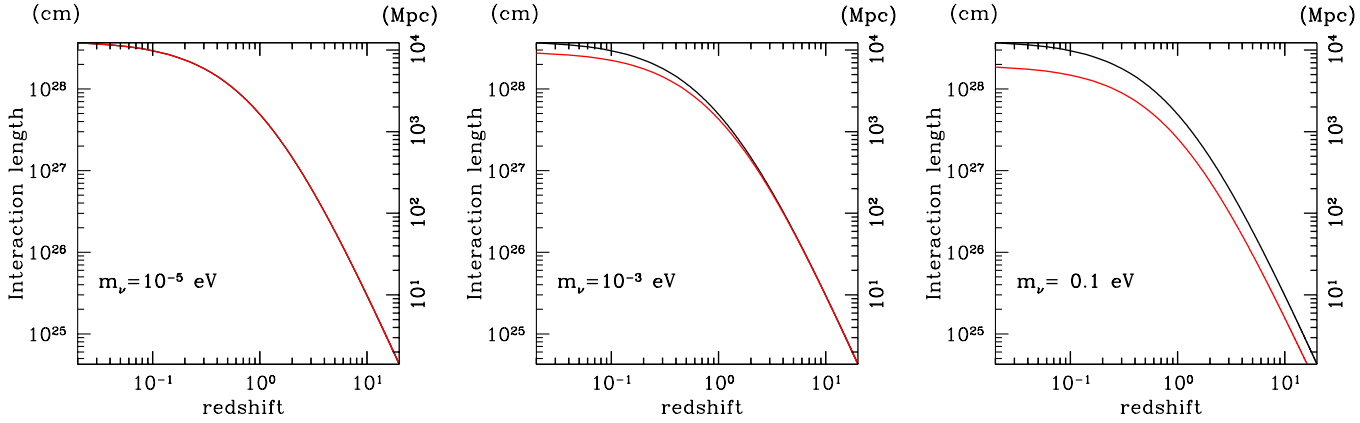

FIG. 8 (color online). Interaction lengths defined in Eq. (27) versus redshift at the Z^0 resonance for neutrino masses $m_\nu = 10^{-5}, 10^{-3}, 10^{-1}$ eV (left, center, and right panels). The left-hand scales are in centimeters, the right-hand scales in megaparsecs (1 Mpc $= 3.085\,678 \times 10^{24}$ cm). In the center and right panels, the lower (black) line is for the Dirac-neutrino case; the upper (red) line applies to Majorana neutrinos.

The interaction length for annihilation on relic neutrinos illustrates the difference between the Majorana and Dirac cases and the transition from static to extreme relativistic regimes. We define

$$\mathcal{L}^{\nu\bar{\nu}}_{\text{int:M,D}} = 1/\sigma_{\text{M,D}}(E_\nu^{\text{Zres}}) n_{\nu_i}(z), \tag{27}$$

where $E_\nu^{\text{Zres}} = M_Z^2/2m_\nu$, and evaluate the ratio (26) using the mean momentum $\langle p_\nu \rangle$ and energy $\langle \varepsilon_\nu \rangle = (\langle p_\nu^2 \rangle + m_\nu^2)^{1/2}$ from the Fermi-Dirac distribution (6). In Fig. 8, we depict the Majorana and Dirac interaction lengths over the range of redshifts considered in this study, for three illustrative values of the relic-neutrino mass.

Contrary to common wisdom, the distinction between Majorana and Dirac relics is not readily observable in neutrino absorption lines, unless the relic-neutrino mass approaches ≈ 0.1 eV, a value close to the present cosmological upper bounds for a quasidegenerate neutrino spectrum. Appreciably lighter relics are relativistic over much or all of the redshift range we consider.

F. Superhigh-energy neutrino sources

1. General orientation

Observing absorption lines on the relic background requires an adequate neutrino flux at the resonant energies $E_\nu^{\text{Zres}} = M_Z^2/2m_{\nu_i} \approx 4.2 \times 10^{21}\ \text{eV}/m_{\nu_i}$. For the sub-eV relics that current information on the neutrino spectrum leads us to expect, the cosmic neutrinos must have energies no less than those of the highest-energy cosmic rays ever observed [68,69]. Indeed, the required cosmic neutrinos have been named *Super-GZK neutrinos* [70], as their energies lie above the Greisen-Zatsepin-Kuzmin [71,72] cutoff in the cosmic-ray spectrum.

It is worth taking a moment to review the GZK argument, because it implies the existence of so-called cosmogenic neutrinos [73]. Extremely high-energy cosmic rays—let us take protons, to be concrete—can lose energy by interacting with the cosmic microwave background whose properties were recalled in Sec. I B. The key energy-loss mechanism is pion photoproduction, $p + \gamma \longrightarrow \pi + N$. Ultrahigh-energy ν_μ, γ, and $\bar{\nu}_\mu$ arise from the decays of π^+, π^0, π^-.

Taking the energy of a typical CMB photon as

$$\langle p_{\gamma 0} \rangle = 3\frac{\zeta(4)}{\zeta(3)} \cdot T_0 \approx 2.701 T_0 \approx 6.341 \times 10^{-4}\ \text{eV}, \tag{28}$$

we estimate the threshold for pion production to be

$$E_p^{\gamma\to\pi} \approx \frac{m_\pi(m_\pi + 2M_p)}{4\langle p_{\gamma 0} \rangle} \approx 1.1 \times 10^{20}\ \text{eV}, \tag{29}$$

where m_π is the pion mass and M_p is the proton mass. Accordingly, any proton with energy $\gtrsim 10^{20}$ eV that traverses a long path in the current Universe will suffer energy loss through pion photoproduction. The interaction length, determined by scattering at the $\Delta(1232)$ resonance, is approximately 10 Mpc, short compared with the 100-Mpc distance to active galaxies. At earlier epochs, the interaction length (at redshifted energy) scales with the number density of CMB photons.

No experiment has yet detected neutrinos with energies above 1 TeV that originate outside Earth's atmosphere. To discuss possible sources[13] of cosmic neutrinos that might be useful for absorption spectroscopy we enter a largely unexplored realm of upper limits and models not disciplined by extensive data sets.

Both acceleration mechanisms and top-down (decay) phenomena may be at the origin of superhigh-energy neutrinos. We consider these two classes of sources briefly in turn.

[13] See the extensive review of cosmic-ray sources in Ref. [74].

Extragalactic objects such as active galactic nuclei and gamma-ray bursters are generally regarded as promising sites for the production of ultrahigh-energy neutrinos. Protons accelerated to extreme energies may collide with the surrounding matter or the bath of photons to produce pions through the inclusive reactions

$$p + (N, \gamma) \rightarrow \pi + \text{anything}. \tag{30}$$

If π^+, π^0, π^- are produced in equal numbers, then the decay chains $\pi^0 \rightarrow \gamma\gamma$ and

$$\pi^+ \rightarrow \mu^+ \nu_\mu \\ \hookrightarrow e^+ \nu_e \bar{\nu}_\mu$$

(and similarly for π^-) imply products in the proportions $\gamma{:}e^+{:}e^-{:}\nu_\mu{:}\bar{\nu}_\mu{:}\nu_e{:}\bar{\nu}_e{::}2{:}1{:}1{:}2{:}2{:}1{:}1$. If such processes were responsible for the flux of ultrahigh-energy gamma rays, then a similar flux of ultrahigh-energy neutrinos would be essentially guaranteed.[14]

The top-down scenarios—superheavy relic particles or topological defects formed in symmetry-breaking phase transitions predicted by unified theories, for example—do not require regions in which astrophysical processes can accelerate particles to superhigh energies, but they depend on physics beyond the standard model that has not been established [79]. They might populate energies beyond the reach of even the most extreme astrophysical processes, conceivably exceeding the scale on which the $\mathrm{SU}(3)_c \otimes \mathrm{SU}(2)_\mathrm{L} \otimes \mathrm{U}(1)_Y$ standard-model interactions are unified.

In this class of models, ultrahigh-energy cosmic rays can be decay products of some supermassive X particles with masses M_X close to the grand unified theory scale. The supermassive X particles could be long-lived relics of the early Universe or could themselves arise from the collapse of topological defects. The X particles can decay into nucleons, gamma rays, and neutrinos with energies approaching M_X.[15] In the simplest models, the fluxes of neutrinos that arise in this manner are bounded by the cascade limit. Hidden-sector topological defects, which may arise in multibrane scenarios, evade the cascade limit and so might provide the largest (which is to say, least constrained) flux of Super-GZK neutrinos [81].

[14]A rather restrictive upper bound (Waxman-Bahcall) follows if energetic protons escape freely from such a source [75]. A more permissive (by $\sim 40\times$) *cascade limit* [76] relates the neutrino flux to the γ-ray flux observed by the EGRET instrument [77] aboard the Compton Gamma-Ray Observatory, assuming the photons are not obscured. Future γ-ray detectors, such as GLAST [78], will improve the photon-flux baseline. In the case of *hidden sources,* from which neither nucleons nor photons escape, there is no way to bound the neutrino flux from above.

[15]See Ref. [80] and the works cited there for a general discussion.

2. Parametrizations of neutrino spectra

Calculation of the cosmogenic neutrino flux is accomplished by propagating an assumed primary proton flux through the cosmic microwave background over the relevant history of the Universe, by means of transport codes. A standard *Ansatz* [80,82] is a power-law shape for the injection spectrum per unit comoving volume,

$$\varphi_p(E, z) = \mathcal{N} \cdot E^{-\alpha}(1+z)^m \Theta(E_\mathrm{max} - E), \tag{31}$$

during the era characterized by $z_\mathrm{min} \leq z \leq z_\mathrm{max}$. Here E_max represents the maximum energy to which protons can be accelerated by astrophysical processes, α is the spectral index, m is the redshift-evolution index, and $\mathcal{N}$ specifies the normalization.

As an example, we show in Fig. 9 ($E_\nu^2 \times$) the cosmogenic neutrino flux $j(E_\nu)$ tuned [80] to saturate the cascade limit, $j(E_\nu)E_\nu^2 \lesssim 450\ \mathrm{eV\,cm^{-2}\,s^{-1}\,sr^{-1}}$, derived from a recent analysis of the EGRET data [83]. As anticipated, the cosmogenic neutrinos lie squarely in the domain of the GZK cutoff on the cosmic-ray spectrum. The flux depicted in Fig. 9 is consistent with direct limits on the neutrino flux, which are summarized in Refs. [23,80]. Equal fluxes (at Earth) of all neutrino flavors is implied by the pattern of neutrino mixing, as we elaborate in the opening paragraphs of Sec. II. We comment briefly on event rates for planned detectors in Sec. III C.

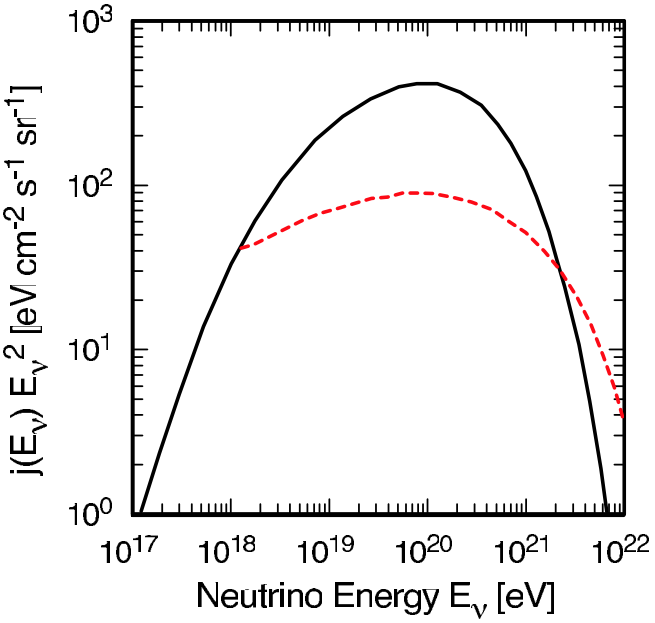

FIG. 9 (color online). Solid line: Maximal cosmogenic neutrino fluxes *per flavor* computed for an injection spectrum characterized by $E_\mathrm{max} = 2 \times 10^{13}$ GeV, $\alpha = 1$, $m = 3$, for $0 \leq z \leq 2$ (from Ref. [80]). Dashed (red) line: Diffuse neutrino flux from hidden topological defects in the form of necklaces, as calculated in Ref. [85] for a superheavy particle of mass $M_X = 10^{14}$ GeV.

To illustrate top-down scenarios, we cite a calculation of the diffuse neutrino flux arising from one species of topological defect, a necklace of monopoles and antimonopoles strung on a cosmic string. Once formed in symmetry-breaking phase transitions in the early Universe, topological defects can survive indefinitely, unless they collapse or annihilate [84], producing massive quanta generically labeled X particles. As monopoles and antimonopoles on a necklace annihilate, they produce X particles in the form of heavy Higgs bosons and gauge bosons. These in turn are the source of ultrahigh-energy cosmic rays and neutrinos; analytic expressions for the fluxes in several cases are computed in Ref. [79].

The dashed (red) curve in Fig. 9 shows the diffuse neutrino spectrum in the present Universe that arises for monopole-antimonopole annihilations into particles with mass $M_X = 10^{14}$ GeV [85]. In top-down scenarios, energetic neutrinos might have been generated at very early times; in that case our computation of the absorption lines will entail an integration over redshift back to those early times.

G. Detectors for cosmic neutrinos

Neutrino astronomy is moving into a new, and much anticipated, era. The value of neutrino observatories has been clearly demonstrated in the MeV range through the detection of neutrinos from Supernova 1987A and from the Sun [86,87]. The detailed observation of atmospheric neutrinos with GeV energies was crucial to establishing neutrino mixing [13], and the AMANDA experiment has detected atmospheric neutrinos up to about 10^5 GeV [88]. Current exploration is dedicated to the search for extraterrestrial neutrinos—either from the diffuse background of active galactic nuclei or from point sources such as gamma-ray bursters—with energies between 10^5 and 10^9 GeV. In addition to the ice-Cherenkov detector AMANDA II, dedicated neutrino telescopes include the BAIKAL water-Cherenkov array [89] and the antenna array RICE [90], which aims to detect radio pulses emitted by neutrino-induced showers in the Antarctic ice. The Fly's Eye [91], HiRes [92], and AGASA [93] air-shower arrays are sensitive to horizontal air showers initiated by neutrino interactions deep in the atmosphere.

The Goldstone lunar ultrahigh-energy (UHE) neutrino experiment (GLUE) [94] has begun to search for radio emission from ultrahigh-energy cascades induced by neutrinos or cosmic rays skimming the moon surface. The FORTÉ (fast on-orbit recording of transient events) satellite [95] has set upper limits on the UHE neutrino fluxes at energies beyond the GZK cutoff, looking for radio pulses generated by neutrino interactions in the Greenland ice sheet.

Over the next few years, significantly increased sensitivities will be attained in IceCube [96], a cubic-kilometer-scale ice-Cherenkov detector evolved from the AMANDA experience that is beginning construction at the South Pole. The ANTARES [97], NEMO [98], and NESTOR [99] projects are developing techniques for a cubic-kilometer water-Cherenkov array in the Mediterranean Sea [100]. It is highly desirable that the next generation of neutrino telescopes not only characterize the incident-neutrino energy and direction, but also tag the neutrino flavor by identifying the outgoing charged lepton. An optimistic assessment of prospects for flavor tagging in detectors such as IceCube can be found in Ref. [101].

ANITA [102], a balloon-borne array of radio antennas, will circle the Antarctic continent at an altitude of $\sim$35 km to record radio bursts from neutrino interactions in the polar ice cap. The Pierre Auger Observatory, a 3000-km^2 hybrid detector for air showers in Argentina's Mendoza province, will be sensitive to the interactions of $\gtrsim 10^9$-GeV neutrinos in the atmosphere [103]. Space-based instruments such as the Extreme Universe Space Observatory (EUSO) [104] and the orbiting wide-angle light collectors [105] would have an energy threshold near 10^{10} GeV.

II. A TOY EXPERIMENT

As a prelude to our investigation of neutrino absorption spectroscopy in the physical Universe, we describe a highly idealized situation in which an extremely high-energy neutrino beam traverses a very long column with the relic-neutrino properties of the current Universe. We neglect for now the expansion of the Universe and the thermal motion of the relic neutrinos. The "cosmic-neutrino attenuator" is thus a column of length L with uniform neutrino density $n_{\nu 0} = 56\ \mathrm{cm}^{-3}$ of each neutrino species, ν_e, $\bar{\nu}_e$, ν_μ, $\bar{\nu}_\mu$, ν_τ, $\bar{\nu}_\tau$.

We imagine a terrestrial detector capable of distinguishing arriving neutrino species through charged-current interactions producing electrons, muons, or tau leptons, and of inferring the energies of the neutrinos that initiated those interactions. A detector of the required scale is unlikely to measure the charge of the outgoing lepton, and so would not distinguish neutrinos from antineutrinos in the beam. Our aim here is to identify the sorts of observations that might be made, should neutrino absorption line spectroscopy become practical, and to point out how various neutrino properties would manifest themselves.

We assume that the incoming neutrino beam originates at least 100 Mpc from Earth, that it contains ν_e, $\bar{\nu}_e$, ν_μ, $\bar{\nu}_\mu$, ν_τ, $\bar{\nu}_\tau$ in sufficient numbers to allow a measurement of the energy spectra of the neutrinos arriving at Earth, and that the neutrino energy spectrum at the source is reasonably smooth.[16] Neutrino oscillations tend to pro-

[16]It is a reasonable bet, though not essential to our analysis, that the beam contains an equal mix of neutrinos and antineutrinos.

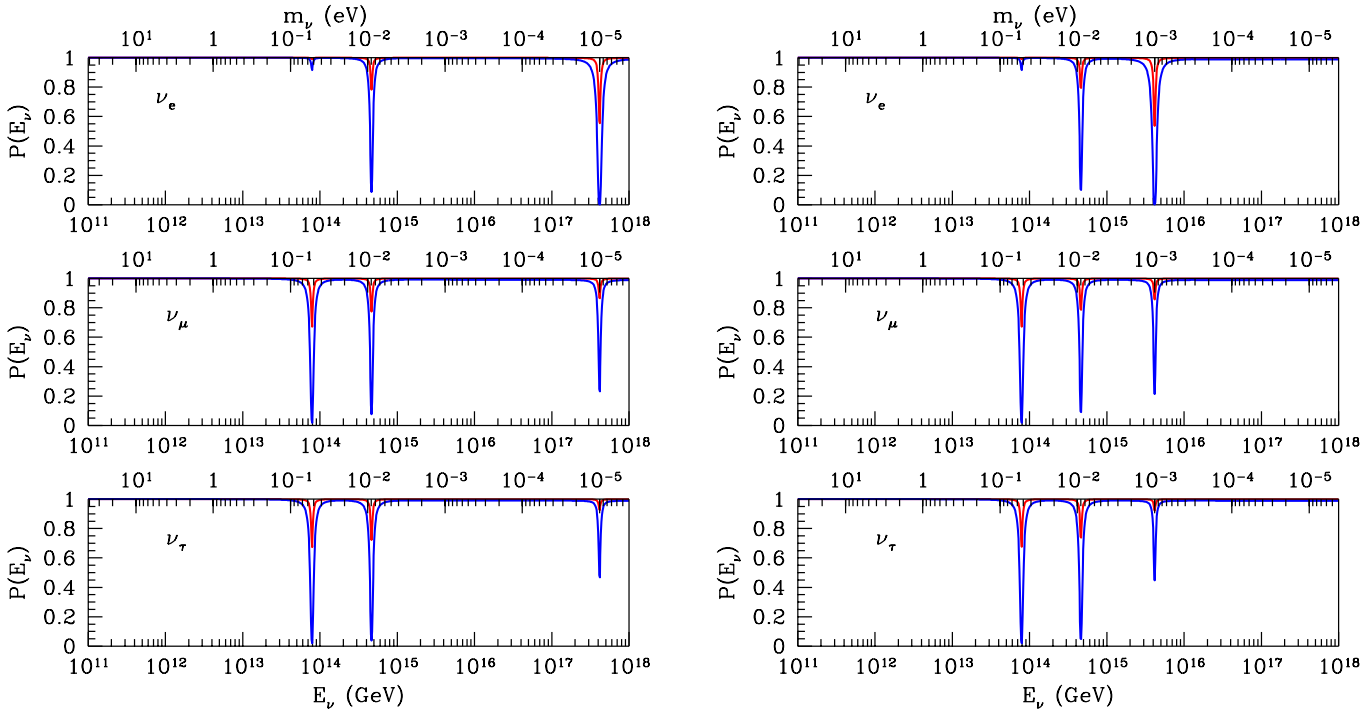

FIG. 10 (color online). Survival probabilities for ν_e, ν_μ, and ν_τ in the ideal experimental scenario, for a normal hierarchy with $m_\ell = 10^{-5}$ eV (left panel) or $m_\ell = 10^{-3}$ eV (right panel). The red and blue curves correspond to $L = 10^4$ and 10^5 Mpc.

duce a "beam" with roughly equal mixtures of ν_e, ν_μ, ν_τ, whatever the flavor mixture of the extremely high-energy neutrinos at the source [106,107]. The vacuum oscillation length, $L_{\rm osc} = 4\pi E_\nu/|\Delta m^2|$, is typically short compared with the intergalactic distances we contemplate. For $|\Delta m^2| = \Delta m^2_{12} \approx 8.2 \times 10^{-5}$ eV^2, for example, the oscillation length is $L_{\rm osc} \approx 3 \times 10^{-25}$ Mpc $\cdot (E_\nu/1$ eV). At the resonance energy $E_\nu^{\rm Zres} = M_Z^2/2m_\nu$, the (solar) oscillation length is thus $L_{\rm osc} \approx 1.2 \times 10^{-3}$ Mpc$/(m_{\nu_i}/1$ eV). Only for the normal hierarchy with $m_\ell \lesssim 10^{-4}$ eV is the oscillation length not a negligible distance. The decoherence length for neutrinos above 10^{18} eV is many orders of magnitude greater than the Hubble distance, $D_H \equiv c/H_0 = 4200$ Mpc$(0.7/h)$ [23].

A. An idealized experiment

As we reviewed in Sec. I C, the mass m_ℓ of the lightest neutrino, which corresponds to m_1 for the normal spectrum or to m_3 for the inverted spectrum, lies between 10^{-5} eV and 0.1 eV. We present here studies for three example values: $m_\ell = 10^{-5}$, 10^{-3}, and 0.1 eV. For a given mass of the lightest neutrino, the graphs in Fig. 5 show our current expectations for the masses of the other neutrinos.

If the column of relic neutrinos is thick enough to attenuate neutrinos appreciably through resonant absorption at the Z^0 gauge boson, the energies that display absorption dips point to the neutrino masses through the condition $m_\nu = M_Z^2/2E_\nu^{\rm Zres}$.[17] Evidently the heaviest neutrino corresponds to the lowest-energy absorption line. For a normal hierarchy, we expect three or two or one absorption lines, as m_ℓ increases; for an inverted hierarchy, two or one absorption lines.

We illustrate this prospect in Fig. 10, where we plot the survival probabilities for ν_e, ν_μ, ν_τ over the relevant range of neutrino energies, for $m_\ell = 10^{-5}$ and 10^{-3} eV. We imagine that the survival probability can be estimated reliably by fitting the shape of the energy spectrum away from the dips, in much the same spirit as backgrounds are estimated in experiments that observe peaks. The amount of attenuation is governed by the length of the column and by the flavor composition of the neutrino mass eigenstates, which was indicated in Fig. 4.

As in other aspects of ultrahigh-energy neutrino studies, flavor tagging at the detector greatly enriches the scientific program [107,109]. With flavor tagging, simply looking for variations in the relative fluxes ν_e/all, ν_μ/all, ν_τ/all with energy may be highly revealing. We plot in Fig. 11 the flux ratios ν_e/ν_μ and ν_τ/ν_μ for normal and inverted hierarchies with $m_\ell = 10^{-5}$ eV.[18] The flavor ratios are a powerful discriminant between the normal and inverted hierarchies, because the ν_e/ν_μ ratio is an excellent diagnostic for the mass eigenstates—even if only the lowest-energy (highest-mass) dip is visible. In the normal hier-

[17] See Ref. [108] for a related strategy to determine the neutrino masses.

[18] We assume the natural mix, ν_e:ν_μ:ν_τ::1:1:1.

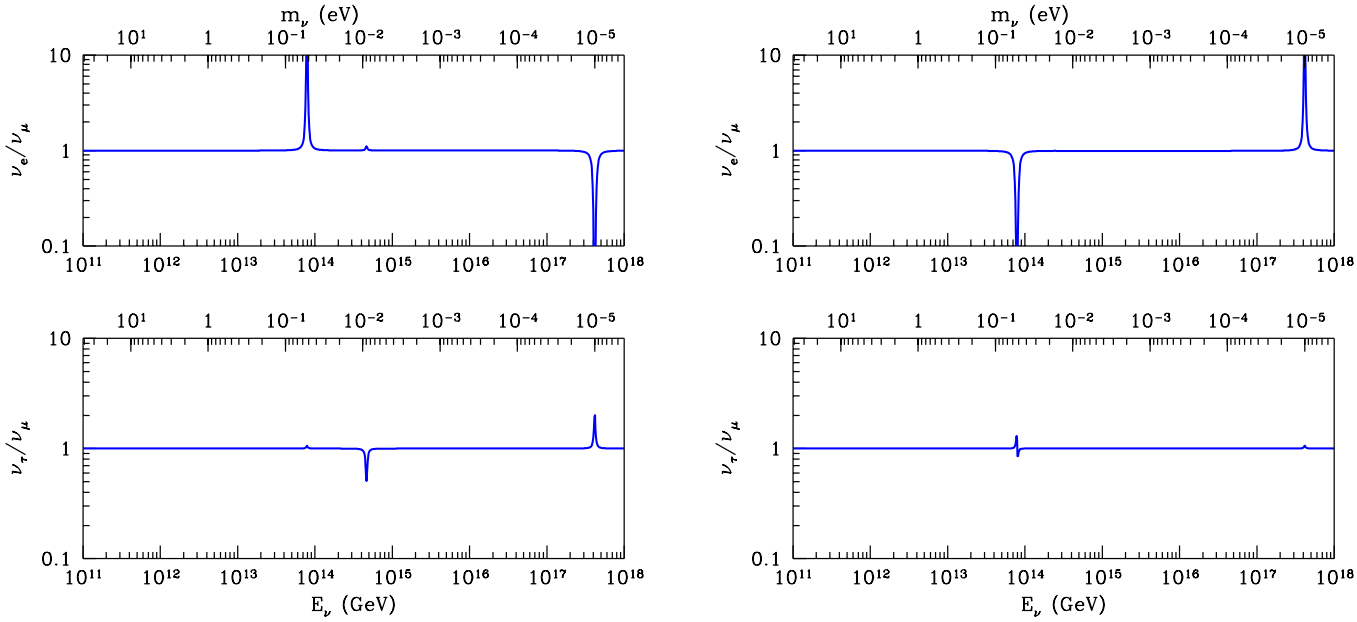

FIG. 11 (color online). Flux ratios ν_e/ν_μ and ν_τ/ν_μ at Earth, for normal (left panel) and inverted (right panel) mass hierarchies with $m_\ell = 10^{-5}$ eV. The column length is $L = 10^5$ Mpc.

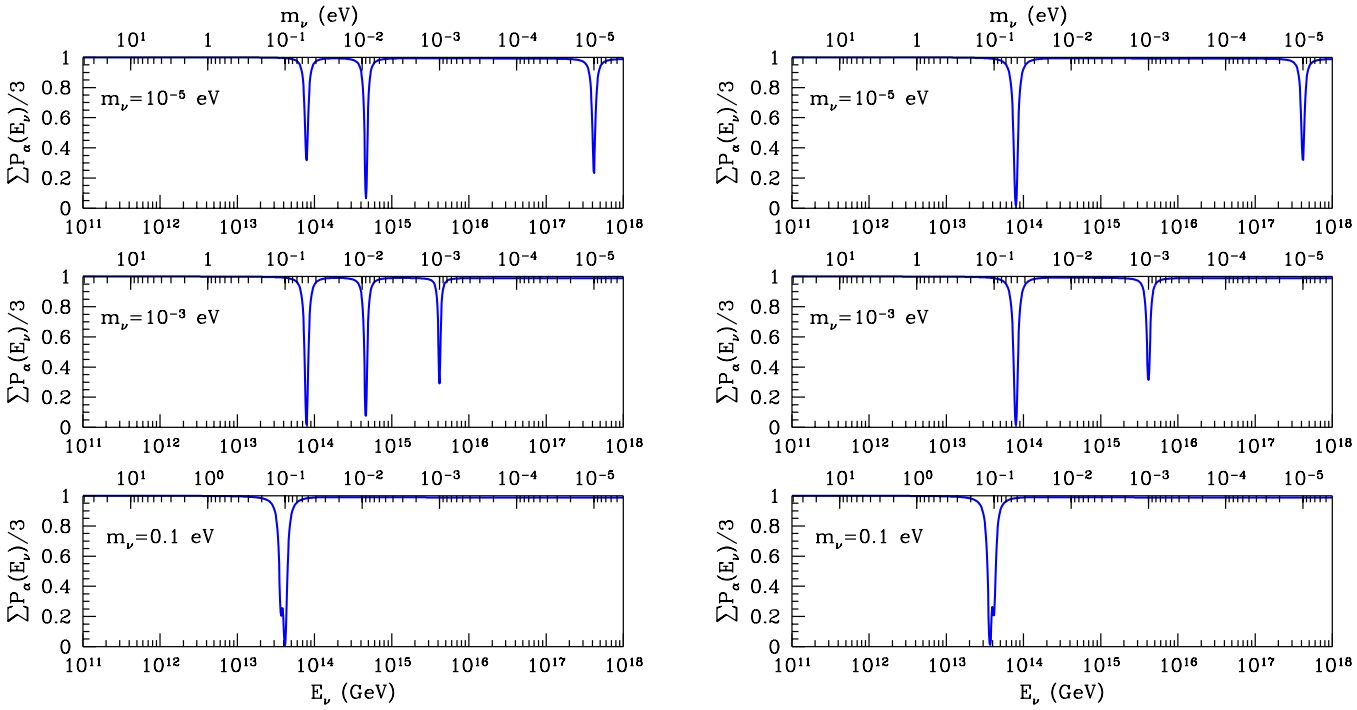

FIG. 12 (color online). Survival probabilities summed over neutrino flavors in the ideal experimental scenario, for $m_\ell = 10^{-5}, 10^{-3}, 10^{-1}$ eV (top, middle, bottom) in the normal (left panel) and inverted (right panel) hierarchy. The length of the relic-neutrino column is $L = 10^5$ Mpc.

archy, muon neutrinos are depleted with respect to electron neutrinos, while for the inverted hierarchy, ν_e is depleted with respect to ν_μ. This distinction can be essential in case the incident-neutrino flux runs out before all of the absorption dips are revealed.

If the neutrino masses exhibit a distinct hierarchy—as is the case for $m_\ell \lesssim 10^{-3}$ eV—then it is possible, with adequate flux, to distinguish the normal and inverted hierarchies, even without flavor identification. In Fig. 12 we show the all-flavor survival probabilities, for a representa-

tive relic-neutrino column length of 10^5 Mpc, for the normal and inverted spectra with $m_\ell = 10^{-5}, 10^{-3}, 10^{-1}$ eV. For the normal hierarchy, we observe three, three, and one absorption lines; for the inverted hierarchy, two, two, and one dips.

B. Majorana or Dirac relics?

We reviewed in Sec. I E the implications of Majorana versus Dirac character for the annihilation cross sections, and showed in Fig. 8 how the distinction depends on neutrino mass and temperature. Absent a calibration of the length of the relic-neutrino column, we do not see how to exploit the factor-of-two difference between Dirac and Majorana cross sections in the static limit to distinguish the two cases. Even in the idealized (zero neutrino temperature) situation we treat in this section, it is hard to imagine inferring the neutrino character from the depth of a single absorption line. If the lightest neutrino were relativistic and the heaviest neutrino nonrelativistic, it is remotely possible to imagine calibrating the effective column density on the highest-energy (lowest neutrino mass) dip, and then noticing a smaller apparent depth for the lowest-energy (highest neutrino mass) dip, in the case of Dirac relics. In the more realistic circumstances we shall describe below, with integration over redshift and attention to the thermal motion of the relics, we do not see how to distinguish Dirac from Majorana relics.

C. Unstable relics

To this point, we have considered neutrinos as stable particles. ''Invisible'' decays, such as the decay of a heavy neutrino into a lighter neutrino plus a very light—or massless—(pseudo)scalar boson such as the majoron [110,111] are not very well constrained by observations [101].[19] If *CPT* invariance holds, SN1987a data set an upper limit on the lifetime of the lightest neutrino of $\tau_\ell/m_\ell \gtrsim 10^5$ s/eV. Observations of solar neutrinos lead to $\tau_2/m_2 \gtrsim 10^{-4}$ s/eV. Finally, if the neutrino spectrum is normal, the data on atmospheric neutrinos coming upward through the Earth, imply $\tau_3/m_3 \gtrsim 10^{-10}$ s/eV. All of these bounds leave open the possibility that heavy relic neutrinos might have long since decayed away, so that the current Universe is filled not with the primordial neutrinos, but with their decay products.[20]

[19]A majoron too massive to serve as a neutrino decay product can nevertheless have important consequences for cosmology, including deviations from the standard expectations for the radiation energy density and changes in the positions of peaks in the cosmic microwave background power spectrum [112].

[20]As we noted in Sec. I C, majoron interactions that would mediate neutrino decays can also mediate (co)annihilations that might lead to a vanishing relic-neutrino density today.

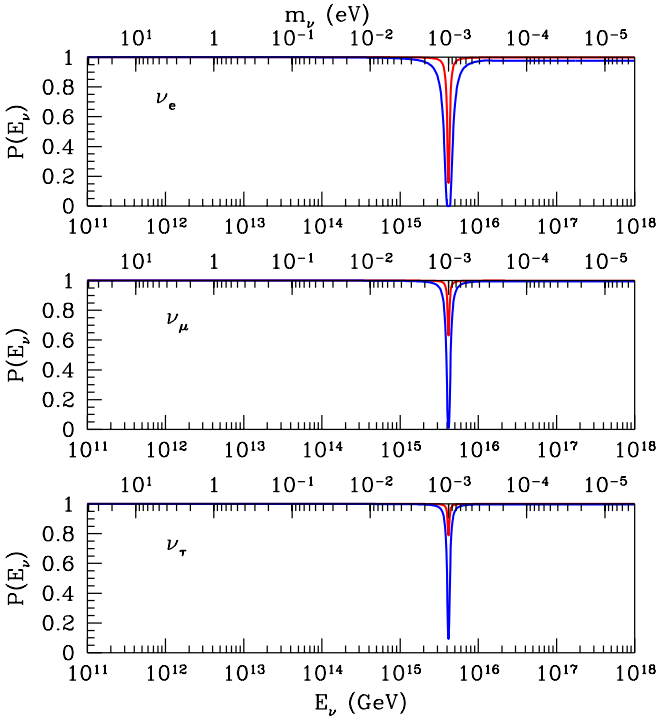

FIG. 13 (color online). Survival probabilities for ν_e, ν_μ, and ν_τ in the idealized experimental scenario, for the normal hierarchy in which all the heavy relics (ν_2 and ν_3) have decayed. The mass of the surviving (lightest) relic is $m_\ell = m_1 = 10^{-3}$ eV. The curves correspond to column lengths $L = 10^4$ Mpc (red) and 10^5 Mpc (blue).

Let us consider, for illustration, the simplest case of unstable neutrinos, in which the two heavier neutrinos have decayed into the lightest neutrino plus invisible products. In that event, the density of the heavier neutrinos is now zero, but the density of the lightest neutrino is 3 times $n_{\nu 0}$. We further assume that the neutrinos in our beam have not decayed in flight. We show in Fig. 13 the neutrino survival probability for the idealized experiment, for the normal hierarchy with $m_\ell = m_1 = 10^{-3}$ eV. In contrast to what we see in the right-hand panel of Fig. 10, there is only one absorption dip located at the resonant energy that corresponds to the lightest neutrino—the surviving relic. The dip is more pronounced for fixed column density than in the standard picture, reflecting the threefold increase in the population of ν_ℓ.[21]

If only the lightest neutrino survives as a relic, the absorption line is necessarily at a higher energy than in the standard case of three surviving flavors. In the extreme case that $m_\ell = 10^{-5}$ eV, the single absorption line would occur at $E_\nu \approx 10^{18}$ GeV, so the demands for adequate flux at the highest energies are very great.

[21]We suppose that all the ν_2 and ν_3 relics have decayed to ν_1, and neglect cosmic expansion.

We note that, with flavor identification, even the single absorption line could signal the normal or inverted hierarchy. In the normal hierarchy, the ν_e flux is strongly absorbed, whereas in the inverted hierarchy it is attenuated only slightly. Without flavor tagging, there is no prospect of unmasking the hierarchy, if the heavy neutrinos are absent as relics.

III. NEUTRINO ABSORPTION LINES IN AN EVOLVING UNIVERSE

Even if we had the means to prepare neutrino beams of the requisite energy, the Universe would not hold still for us to perform the idealized measurements described in Sec. II. The time required to traverse one interaction length for $\nu\bar{\nu} \to Z^0$ annihilation on the relic background in the current Universe (1.2×10^4 Mpc = 39 Gly) exceeds the age of the Universe,[22] not to mention the human attention span. If we are ever to detect the attenuation of neutrinos on the relic-neutrino background, we shall have to make use of astrophysical or cosmological neutrinos sources traversing the Universe over cosmic time scales. The expansion of the Universe over the propagation time of the neutrinos entails two important effects: the evolution of relic-neutrino density and the redshift of the incident-neutrino energy. We consider both effects in this section.

A. The influence of expansion and redshift

We displayed the redshift dependence of the relic-neutrino number density in Fig. 2 in Sec. I B. There we also introduced the column density defined in Eq. (14) and plotted in Fig. 3, which characterizes the neutrino number density per unit of redshift.

As we look back in time, the present energy $E_{\nu 0}$ of an ultrahigh-energy neutrino increases with redshift as $E_\nu(z) = (1 + z)E_{\nu 0}$. This scaling is easily understood: the energy of an ultrarelativistic particle is inversely proportional to its wavelength, which stretches out in an expanding Universe as $(1 + z)^{-1}$.

We evaluate the survival probabilities as

$$\mathcal{P}(E_{\nu 0}) = \exp\left[- \int_0^z dz \sigma_{\nu\nu}((1 + z)E_{\nu 0}) \frac{d\bar{n}_{\nu_i}(z)}{dz} \right], \quad (32)$$

where $\sigma_{\nu\nu}$ is the interaction cross section of Sec. I D weighted with the appropriate mass-flavor mixing factor and $d\bar{n}_{\nu_i}/dz$ is the column density, Eq. (14).[23] The attenuation process is thus summed over redshift, with the simplifying assumption that the neutrino sources in question switched on at a time in the past characterized by a single redshift, which we take to be $z_\nu \lesssim 20$.

[22] Some 13 Gly according to the current best estimates.

[23] We choose not to smear the cross section over a neutrino spectrum, to make our analysis as generally informative as possible. Equation (32) would result for any power-law neutrino spectrum.

Plausible acceleration sources of ultrahigh-energy neutrinos, including active galactic nuclei and gamma-ray bursters, lie at redshifts of a few [80]. Extremely energetic neutrinos might have been generated in the decays of superheavy particles or topological defects [79,80,85,113] long before the first stars began to shine. Their interaction with the relic-neutrino background could reach as far back as the epoch of light-neutrino decoupling, $z \sim \mathcal{O}(10^{10})$ [21].

We show in Fig. 14 the survival probabilities for ν_e, ν_μ, ν_τ integrated from the present back to redshift $z = 20$, for $m_\ell = 10^{-5}$ and 10^{-3} eV. Comparing with the analogous idealized "toy experiment" whose outcome was depicted in Fig. 10, we find that the absorption dips are distorted by the redshift of neutrino energies. Neutrino-antineutrino annihilation into Z^0 at redshift z implies a depletion of neutrino flux now at an energy

$$E_{\nu 0}^{\mathrm{Zres}:z} = \frac{M_Z^2}{2m_{\nu_i}(1 + z)}. \quad (33)$$

The correspondence between neutrino mass and energy of an absorption line is compromised. No longer does the unredshifted relation $m_\nu = M_Z^2/2E_\nu^{\mathrm{Zres}}$ allow the neutrino mass to be inferred reliably. In these examples, that simple relation would overestimate neutrino masses by about an order of magnitude. In compensation, moving the dips to lower energies may be an important advantage for an experiment that is almost sure to be flux-limited.

If terrestrial experiments determine the neutrino masses—or if other considerations place increasingly stringent bounds on the neutrino masses—then the location of the neutrino absorption lines might provide new information about the neutrino sources. If, for example, the location of the dip lies much more than 1 order of magnitude below the anticipated energy, that would be strong evidence that sources of extremely high-energy neutrinos existed before the stars—a surprising and important conclusion.

The morphology of the distortion is illustrated in Fig. 15, where we plot the ν_e survival probability binned in redshift for the simple (one-dip) case of a degenerate neutrino spectrum with $m_\ell = 0.1$ eV. Evidently binning in redshift is not an observational possibility, but we can impose it on our calculation to deconstruct the origin of the shift and broadening of the absorption line. As expected, we observe that the downward shift in the attenuated energy in the present Universe grows with the redshift at which the annihilation occurred. Moreover, the depth of the absorption dips is greater at higher redshifts, because of the increased column density of relic neutrinos, Eq. (14).

In an evolving Universe, the neutrino flux ratios remain an effective discriminant of the mass hierarchy. Figure 16 shows the survival probabilities for an inverted spectrum with $m_\ell = 10^{-5}$ eV. We plot in Fig. 17 the flux ratios ν_e/ν_μ and ν_τ/ν_μ for normal and inverted hierarchies

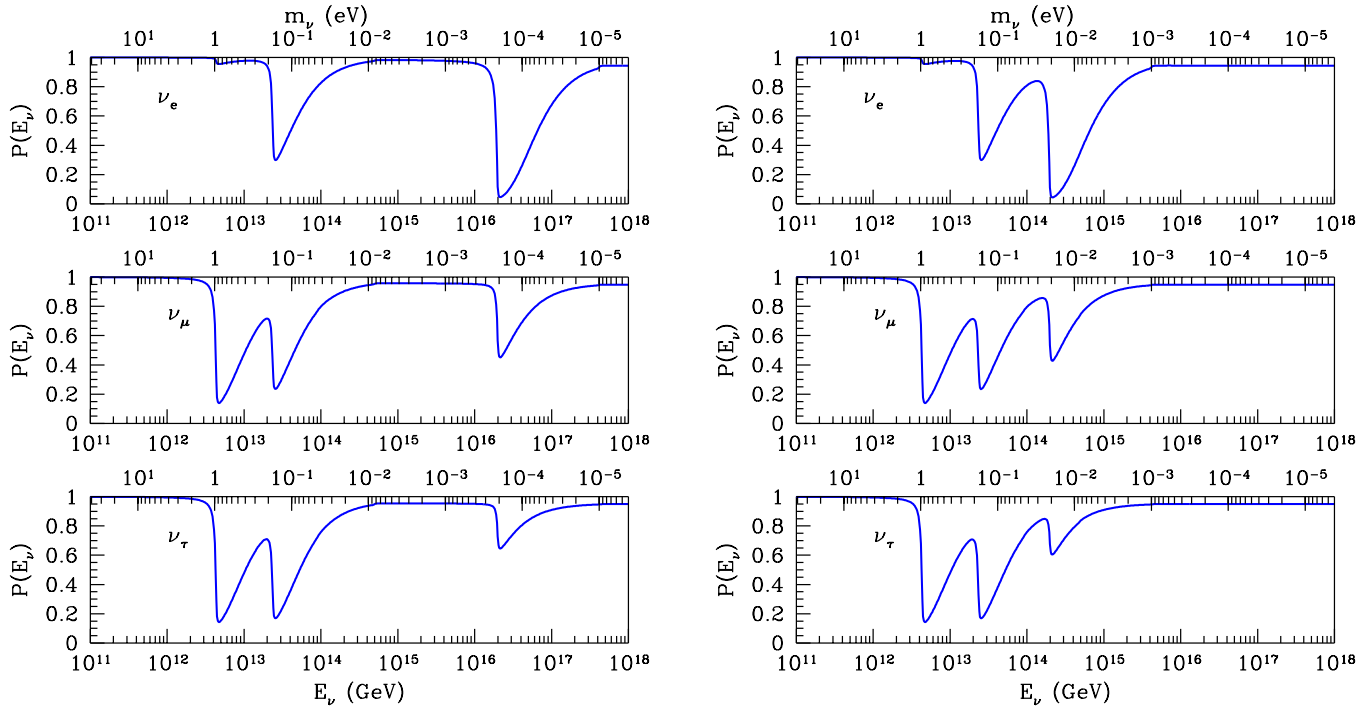

FIG. 14 (color online). Survival probabilities for ν_e, ν_μ and ν_τ after an integration back to redshift $z = 20$, for a normal hierarchy with $m_\ell = 10^{-5}$ eV (left panel) or $m_\ell = 10^{-3}$ eV (right panel), as a function of the energy of the UHE neutrino. The scale at the top shows the neutrino mass defined as $m_\nu = M_Z^2/2E_\nu$ that would be inferred if neutrino energies were not redshifted.

with $m_\ell = 10^{-5}$ eV, integrated back from the present to redshift $z = 20$. Compared with the toy-model ratios plotted in Fig. 11, the features are broadened and displaced toward lower energies, but the essential message is unchanged. In the normal hierarchy, $\nu_e/\nu_\mu > 1$ at the lowest-energy line, whereas in the inverted hierarchy $\nu_e/\nu_\mu < 1$.

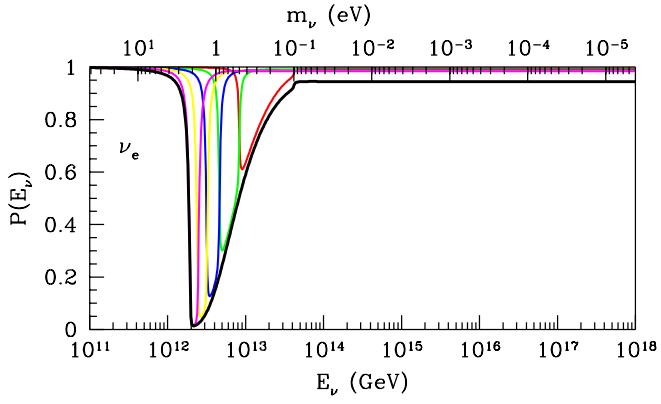

FIG. 15 (color online). Electron-neutrino survival probabilities integrated back to $z = 20$ for a degenerate neutrino spectrum with $m_\ell = 0.1$ eV. The thick black curve shows the distorted absorption line after integration back to redshift $z = 20$, and the colored lines (from right to left) show the contributions from bins in redshift: red, $0 \le z \le 4$; green, $4 \le z \le 8$; blue, $8 \le z \le 12$; yellow, $12 \le z \le 16$; magenta, $16 \le z \le 20$.

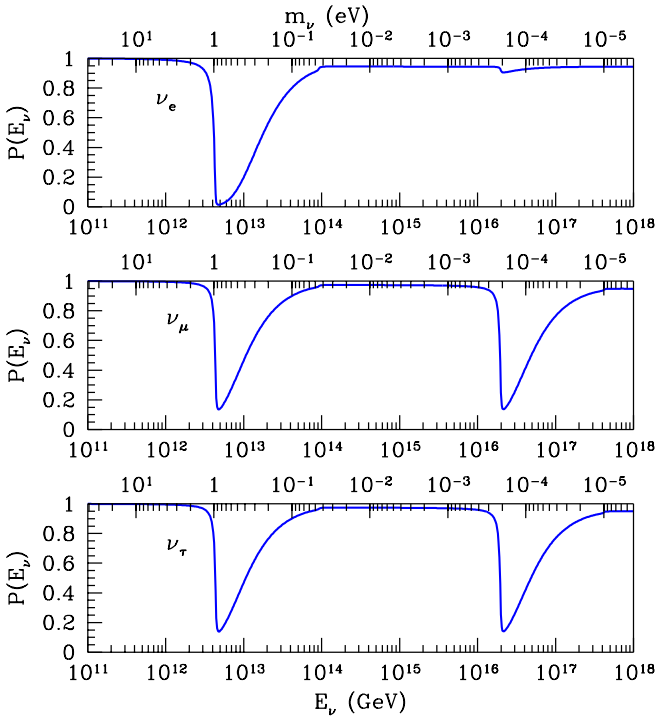

FIG. 16 (color online). Survival probabilities for ν_e, ν_μ and ν_τ after an integration back to redshift $z = 20$, for an inverted hierarchy with $m_\ell = 10^{-5}$ eV, as a function of the energy of the UHE neutrino. The scale at the top shows the neutrino mass defined as $m_\nu = M_Z^2/2E_\nu$ that would be inferred if neutrino energies were not redshifted.

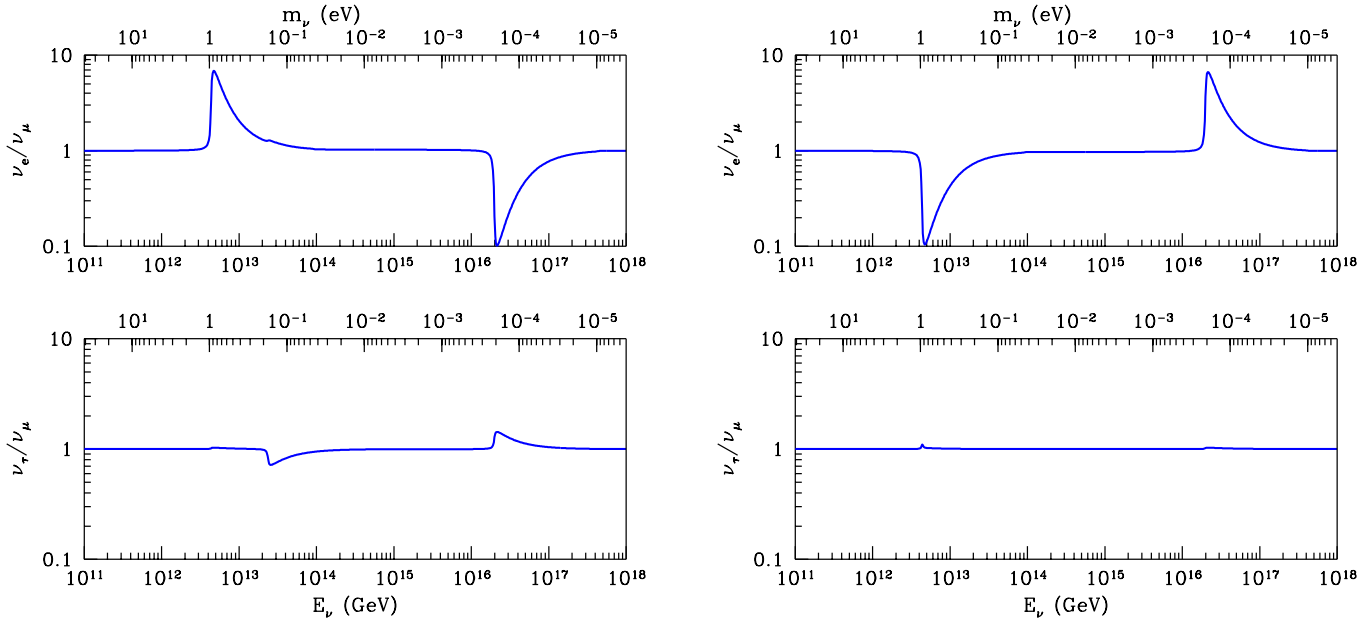

FIG. 17 (color online). Flux ratios ν_e/ν_μ and ν_τ/ν_μ at Earth, for normal (left panel) and inverted (right panel) mass hierarchies with $m_\ell = 10^{-5}$ eV, after integration back to redshift $z = 20$. The scale at the top shows the neutrino mass defined as $m_\nu = M_Z^2/2E_\nu$ that would be inferred if neutrino energies were not redshifted.

B. Alternative thermal histories

Since the redshift dependence of the relic-neutrino column density is imprinted on the neutrino absorption lines, it might be possible to infer some information about the column density from the absorption line shape. As we saw in the discussion surrounding Eqs. (12)–(14), each particular cosmology influences the relic-neutrino column density through the Hubble parameter (13).

We have adopted the ΛCDM model as our standard reference cosmology. Let us compare its implications for neutrino absorption lines with those of its predecessor, the SCDM (for standard cold dark matter) model characterized by matter density $\Omega_m = 1$ and zero cosmological constant.

In Fig. 18 we compare the relic-neutrino column densities for these two cosmological models. The column density is systematically larger in the ΛCDM model, because flat-Universe models with a cosmological constant imply a larger physical volume associated with unit redshift than flat-Universe models dominated by matter. As Fig. 19 shows, neutrino attenuation is more efficient in the ΛCDM model than in the SCDM model. There, as in Fig. 15, we show our expectations for the ν_e survival probabilities integrated back to $z = 20$, for a degenerate neutrino spectrum with $m_\ell = 0.1$ eV.

If we had a "standard candle" for neutrinos analogous to the type Ia supernovas for photons, we might imagine discriminating between these two cosmological models, because the difference we compute here is similar to what is revealed by the supernova luminosity distances. Just as distant supernovas appear fainter in a dark-energy dominated Universe, so are the extremely high-energy neutrinos more thoroughly absorbed.

The discrimination among cosmological models would be more acute if extremely high-energy neutrino creation—and attenuation—were initiated at much earlier times, or much larger redshifts, than we consider in this example. If supermassive particle decays are an addi-

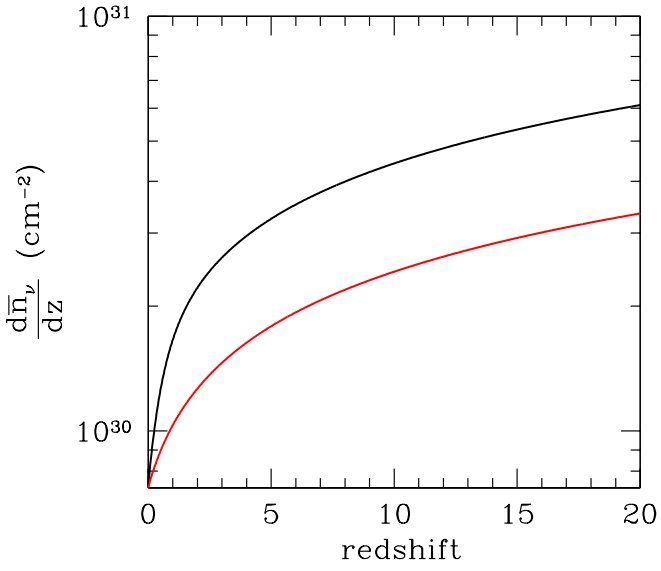

FIG. 18 (color online). Relic-neutrino column densities versus redshift for the ΛCDM model (upper black curve) and SCDM model (lower red curve).

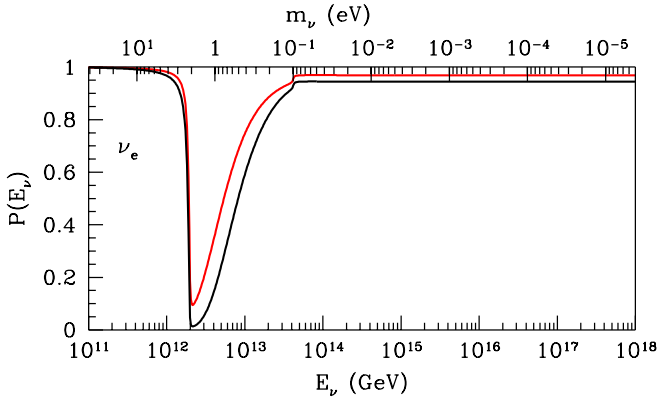

FIG. 19 (color online). Electron-neutrino survival probabilities integrated back to $z = 20$ for a degenerate neutrino spectrum with $m_\ell = 0.1$ eV in the ΛCDM model (lower black curve) and SCDM model (upper red curve).

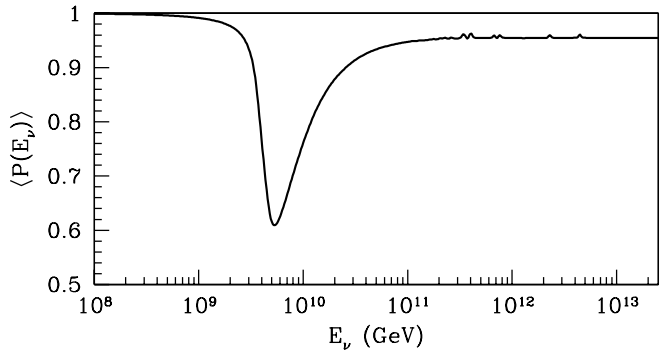

FIG. 20. Survival probability for electron neutrinos created in the decay of a superheavy particle, X, with $M_X = 10^{14}$ GeV, for the case of $m_\ell = 0.1$ eV.

tional—early—neutrino source, then different thermal histories might yield dramatically different neutrino absorption lines.

C. Event rates

Since experiments have just begun to explore the spectrum of ultrahigh-energy neutrinos, quantifying the challenge of establishing neutrino absorption lines is a very uncertain undertaking. We refer to Sec. III of Ref. [23] for a useful assessment. We concur that observing the cosmic-neutrino absorption lines with planned detectors will require extended exposures, exotic sources of ultrahigh-energy neutrinos, or both. Here we briefly examine the case of quasidegenerate neutrino masses, which minimizes the energy required of the incoming neutrinos.

Neutrino absorption lines in the flux of cosmogenic neutrinos will appear at neutrino energies $E_\nu \gtrsim 10^{12}$ GeV, whereas those in the flux of neutrinos generated much earlier from topological defects may be redshifted to energies $E_\nu \lesssim 10^{10}$ GeV. Such energies lie in the domain of radio-Cherenkov and air-shower detectors [114]. IceCube is optimized for neutrinos in the TeV-to-PeV range; it is sensitive to neutrinos of much higher energies, though the ability to characterize the neutrino energy diminishes progressively. IceCube and possible extensions [115] hold promise for identifying the flavor of the ultrahigh-energy neutrinos. We explore here the expected sensitivities to the absorption lines in the future ANITA mission [102].

Suppose now that superhigh-energy neutrinos arise from the decay of superheavy particles created in the collapse (or annihilation) of topological defects. If these neutrinos are produced at very early times, detecting their annihilation on the relic-neutrino background may give us a rare glimpse of processes that prevailed in the very early Universe. For example, the monopole-antimonopole boundstates dubbed "monopolonium" would have formed at the time of helium synthesis [84]. Neutrinos released in the decay of X particles, as described in Sec. I F 2, have traversed many different epochs; the expansion of the Universe during the neutrino's propagation will be imprinted on the neutrino spectrum. It remains to be seen whether we can learn to read the imprints in the absorption lines.

We show in Fig. 20 the survival probability for neutrinos emitted in the decay of 10^{14}-GeV X particles, following Ref. [79]. For a degenerate neutrino spectrum, the absorption line occurs at $E_\nu \lesssim 10^{10}$ GeV, well within the range to be covered by future experiments, including ANITA and EUSO. In the most optimistic scenario for the topological-defect neutrino fluxes, a 5-σ significance level (164 events) could be achieved after a single 15-day flight of ANITA [102]. For these redshifted, early-time neutrinos, we must face an additional complication: the presence of relatively late-time neutrino sources, such as the cosmogenic mechanism, that provide a pedestal under the signal. If the foreground sources are too bright, compared to the flux from top-down sources, more events will be needed to establish the absorption lines.

IV. EFFECT OF THE RELIC-NEUTRINO TEMPERATURE

Relic neutrinos are moving targets, with their momentum distribution characterized in the present Universe by Eq. (6). The thermal motion of the neutrinos gives rise to a Fermi (momentum) smearing of the UHE-ν–relic-ν cross section. The resonant incident-neutrino energy for a relic neutrino in motion is given by

$$E_\nu^{\rm Zres} = \frac{M_Z^2}{2(\varepsilon_\nu - p_\nu \cos\theta)}, \tag{34}$$

where p_ν and ε_ν are the relic-neutrino momentum and energy. The angle θ characterizes the direction of the relic neutrino with respect to the line of flight of the incident

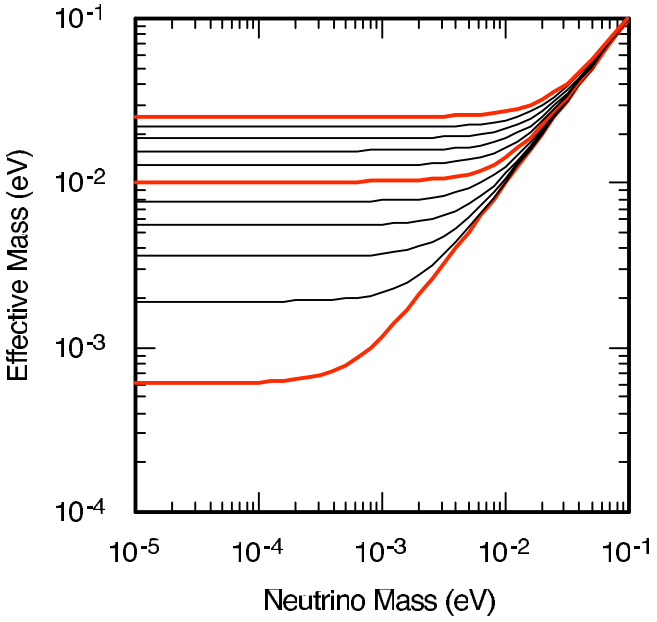

FIG. 21 (color online). Effective masses of relic neutrinos, estimated by $\varepsilon_\nu = [\langle p_\nu^2\rangle + m_\nu^2]^{1/2}$, as functions of the neutrino mass m_ν. The mean-squared neutrino momentum in the current Universe is given by Eq. (10). From bottom to top, the curves refer to redshifts z from 0 to 20, in steps of 2.

UHE neutrino. Accordingly, the resonant energy will be displaced downward from $M_Z^2/2m_\nu$ to approximately

$$\tilde{E}_\nu^{\mathrm{Zres}} = \frac{M_Z^2}{2\langle\varepsilon_\nu\rangle}, \tag{35}$$

where $\langle\varepsilon_\nu\rangle = [\langle p_\nu^2\rangle + m_\nu^2]^{1/2}$ plays the role of an *effective relic-neutrino mass*. We plot the effective mass in Fig. 21, for the interesting range of neutrino masses and redshifts.

The root-mean-square relic-neutrino momentum, which ranges from 6×10^{-4} eV in the present Universe to 2.5×10^{-2} eV at redshift $z = 20$, thus serves as a rough lower bound on the effective neutrino mass. At a given redshift, the resonance peak for scattering from any neutrino with $m_\nu \lesssim \langle\varepsilon_\nu\rangle$ will be changed significantly.

We display the effect of Fermi motion on the Z^0-formation cross section in Fig. 22. The annihilation cross section depends on the relic-neutrino energy and momentum. We have integrated the exact expression for the cross section weighted with the Fermi-Dirac momentum distribution of the relic neutrinos over the relic-neutrino momentum phase space. We show two series corresponding to redshifts $z = 0$ and 20 and relic-neutrino masses 10^{-5}, 10^{-4}, 10^{-3}, 10^{-2}, and 10^{-1} eV. In each panel, the narrow peak (red curve) shows the annihilation cross section as a function of incident-neutrino energy for a stationary relic-neutrino target; the broad peak (blue curve) shows the annihilation cross section averaged over the thermal distribution of relic-neutrino momenta. In every case, the thermally averaged cross section peaks near $\tilde{E}_\nu^{\mathrm{Zres}}$, indicated by a downward arrow. Consequently, the neutrino mass inferred from the location of an absorption line in a hypothetical experiment at fixed redshift would be approximately $\langle\varepsilon_\nu(z)\rangle$, rather than the true neutrino mass, whenever $\langle\varepsilon_\nu(z)\rangle \gtrsim m_\nu$.

Now we consider the influence of thermal motion on the structure of neutrino absorption lines in an evolving Universe, integrating over redshift as we did in

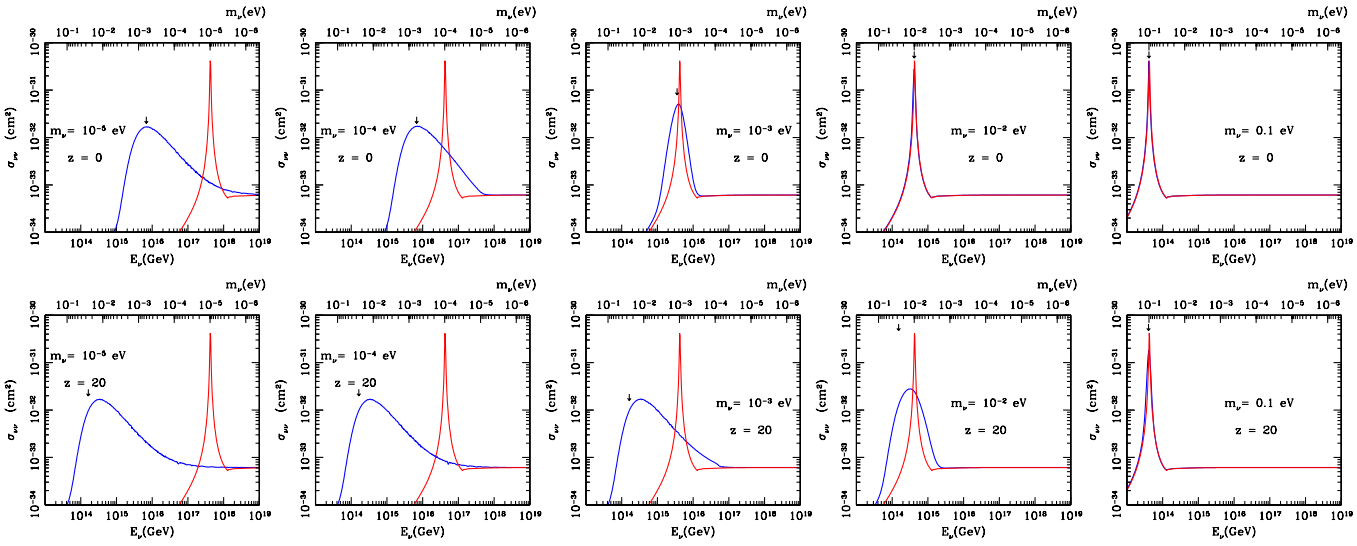

FIG. 22 (color online). Neutrino-antineutrino (annihilation) cross section as a function of the incident-neutrino energy. In each panel, the narrow peak (red curve) applies for a relic neutrino at rest. The broader (blue) curves, shifted to lower energies result when the Fermi motion of the thermal distribution of relic neutrinos is taken into account. The upper series corresponds to relics in the present Universe ($z = 0$); the lower series corresponds to redshift $z = 20$. From left to right, the panels depict relic-neutrino masses 10^{-5}, 10^{-4}, 10^{-3}, 10^{-2}, and 10^{-1} eV. Arrows designate the thermally displaced resonant energy $\tilde{E}_\nu^{\mathrm{Zres}}$ given by Eq. (35).

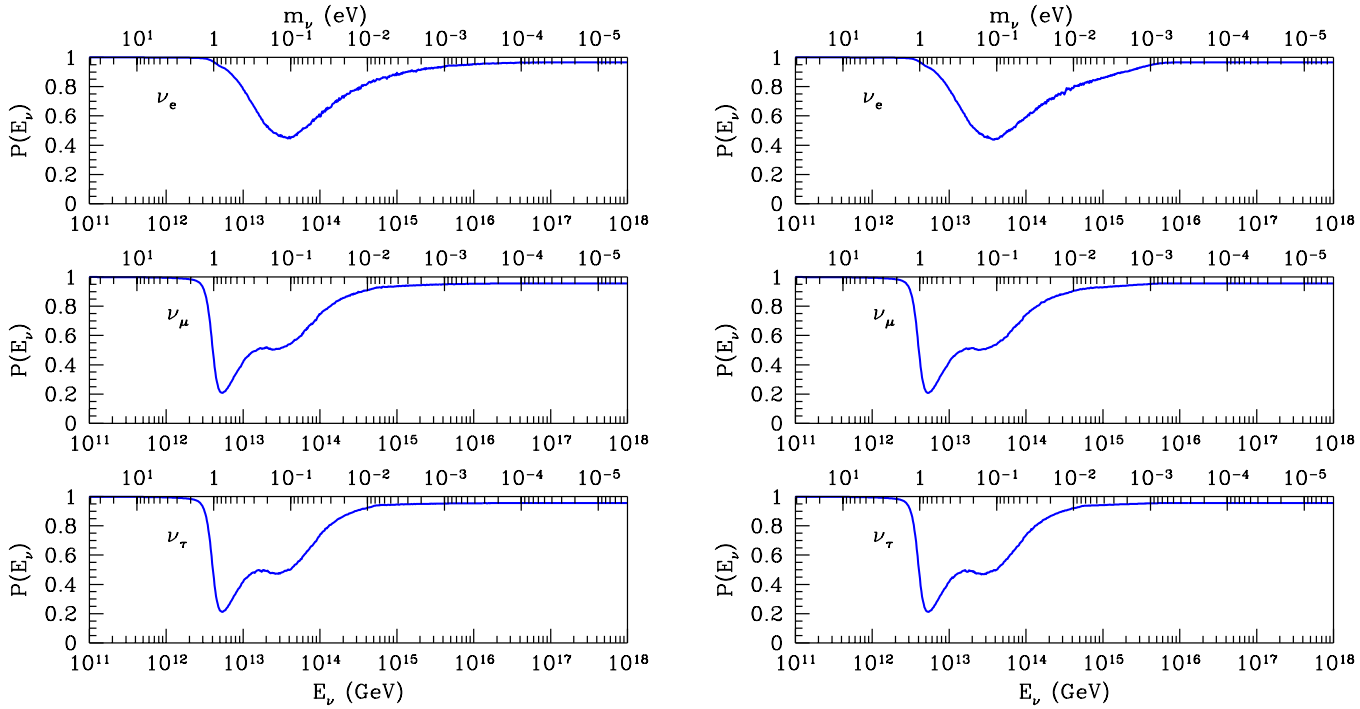

FIG. 23 (color online). Survival probabilities for ν_e, ν_μ, and ν_τ as a function of the neutrino energy, after integration back to redshift $z = 20$, taking into account the Fermi smearing induced by the thermal motion of the relic neutrinos. The results apply for a normal hierarchy with lightest neutrino mass $m_\ell = 10^{-5}$ eV (left panel) or $m_\ell = 10^{-3}$ eV (right panel).

Sec. III A. We show in Fig. 23 the survival probabilities for ν_e, ν_μ, ν_τ integrated from the present back to redshift $z = 20$, for $m_\ell = 10^{-5}$ and 10^{-3} eV. Comparing with the analogous calculation neglecting the Fermi motion of the relic neutrinos, whose outcome was depicted in Fig. 14, we find that the three distinct dips have been merged into a single complex dip. As we could anticipate from the displacement of the resonant energies displayed in Fig. 22, the prospect of determining distinct absolute neutrino masses has faded appreciably.

The distinction between the normal and inverted hierarchy remains, however. We plot in Fig. 24 the survival probabilities in the case of an inverted hierarchy with $m_\ell = 10^{-5}$ eV. Again, Fermi motion has merged the two distinct absorption lines (compare Fig. 16) into one. The pattern of ν_e, ν_μ attenuation is different from the normal-hierarchy case, as we show in Fig. 25. In the normal-hierarchy case, $\nu_e/\nu_\mu > 1$ for the prominent dip at the lowest energy, whereas for the inverted hierarchy $\nu_e/\nu_\mu < 1$.

Although the thermal motion of the relics is largely responsible for obliterating the three-dip structure, we might inquire whether some of the structure would survive if the sources of ultrahigh-energy neutrinos came into existence more recently than redshift $z = 20$. In Fig. 26 we show the survival probabilities for normal and inverted hierarchies, with the lightest neutrino mass $m_\ell = 10^{-5}$ eV, integrating from the present back to redshift $z = 10$. The multiple dip structure is somewhat more pronounced than

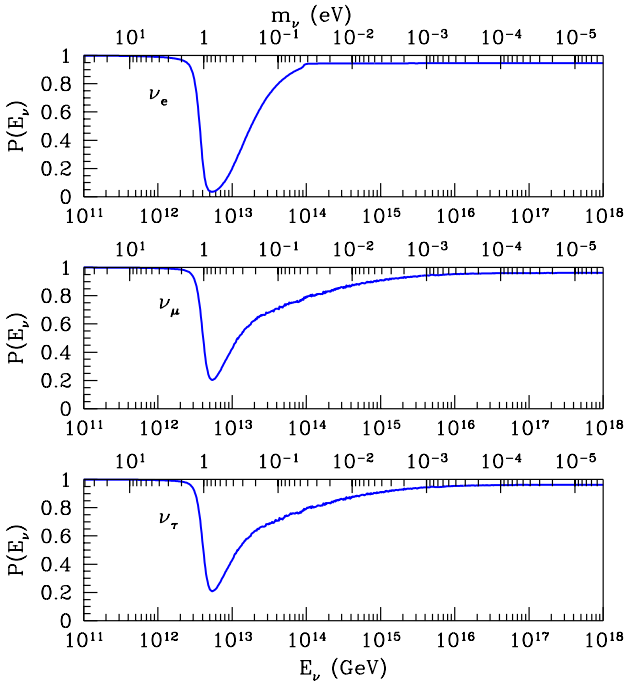

FIG. 24 (color online). Survival probabilities for ν_e, ν_μ, and ν_τ as a function of the neutrino energy, after integration back to redshift $z = 20$, taking into account the Fermi smearing induced by the thermal motion of the relic neutrinos. The results apply for an inverted hierarchy with lightest neutrino mass $m_\ell = 10^{-5}$ eV.

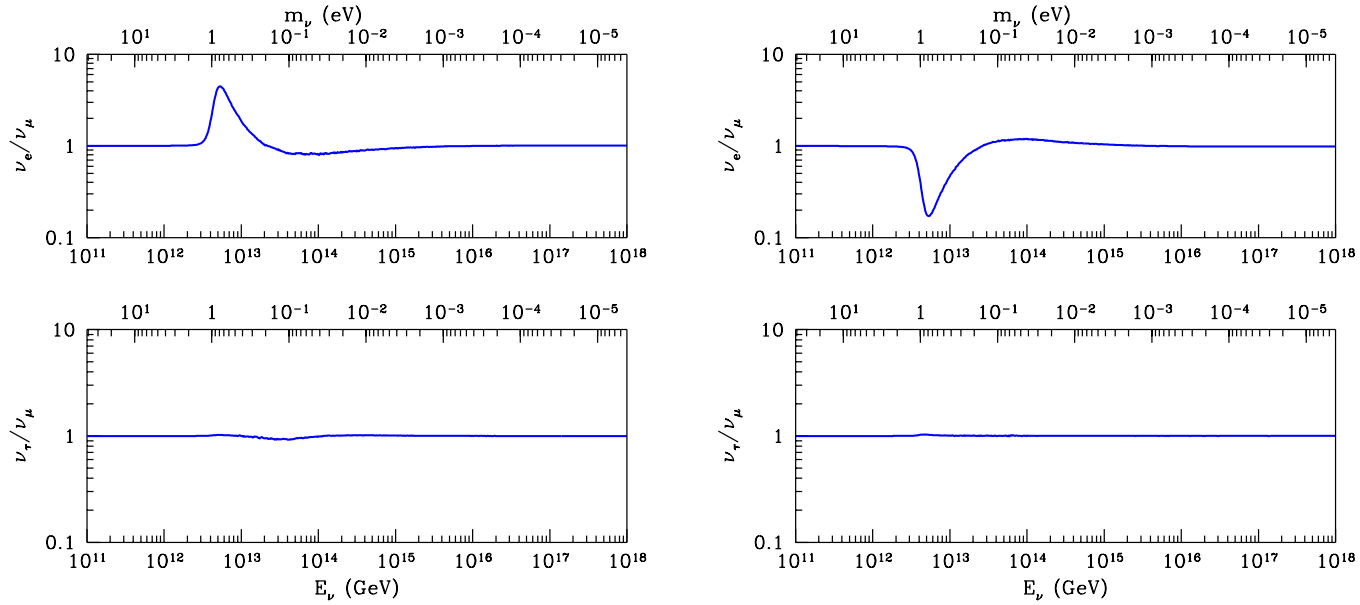

FIG. 25 (color online). Flux ratios ν_e/ν_μ and ν_τ/ν_μ at Earth, for normal (left panel) and inverted (right panel) mass hierarchies with $m_\ell = 10^{-5}$ eV, after integration back to redshift $z = 20$ and a thermal averaging over the relic-neutrino momentum distribution. The scale at the top shows the neutrino mass defined as $m_\nu = M_Z^2/2E_\nu$ that would be inferred if neutrino energies were not redshifted.

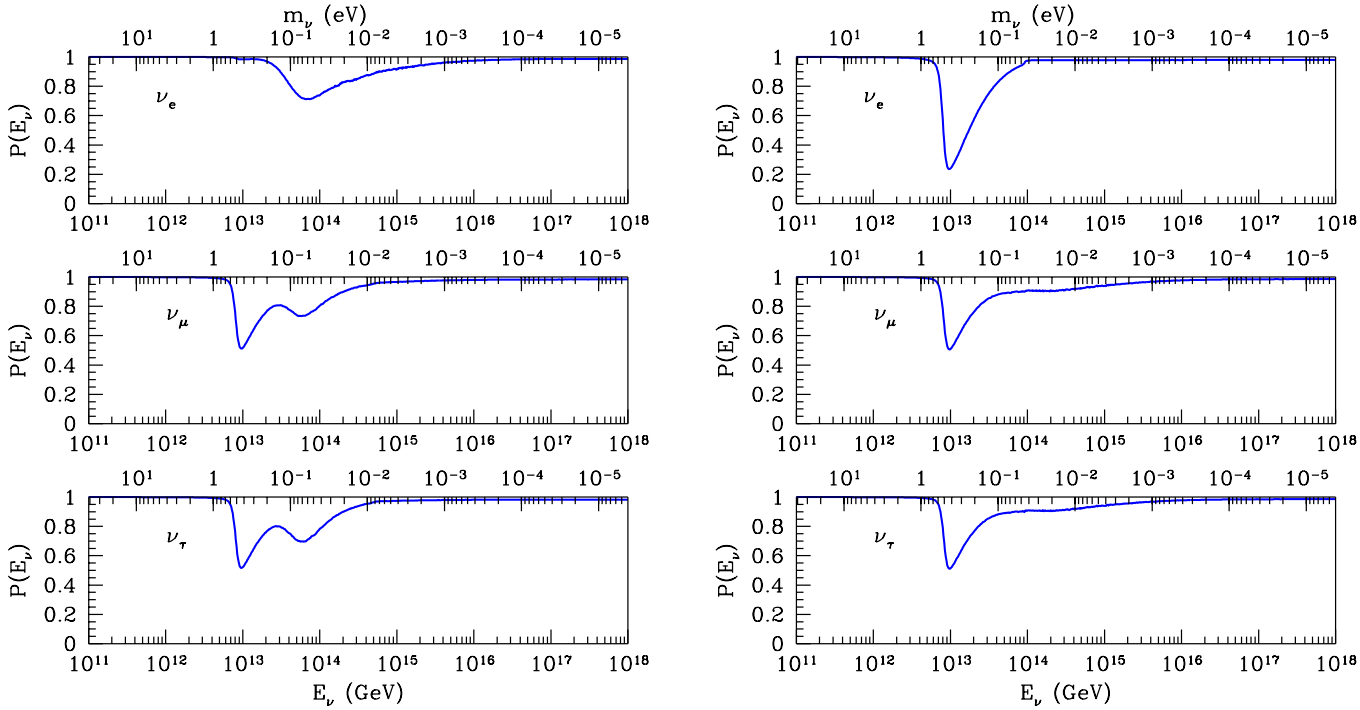

FIG. 26 (color online). Survival probabilities for ν_e, ν_μ, and ν_τ as a function of the neutrino energy, after integration back to redshift $z = 10$, taking into account the Fermi smearing induced by the thermal motion of the relic neutrinos. The results apply for a normal hierarchy (left panel) or inverted hierarchy (right panel), with lightest neutrino mass $m_\ell = 10^{-5}$ eV.

in the $z = 20$ scenario, but still indistinct. Because the Universe is more transparent to neutrinos when evolved back through $z = 10$ than evolved back through $z = 20$, the dips are less prominent than in Figs. 23 and 24. Flux ratios again distinguish the normal and inverted hierarchies.

V. UNCONVENTIONAL NEUTRINO HISTORIES

A. Lepton asymmetry in the early Universe

If the number of leptons differed from the number of antileptons in the early Universe, the present density of relic neutrinos might be very different from the expected value of $56\,\mathrm{cm}^{-3}$. In the standard big-bang model, the neutrino asymmetry $\eta_{\nu_\alpha} \equiv (n_{\nu_\alpha} - n_{\bar{\nu}_\alpha})/n_\gamma$, is assumed to be negligibly small, comparable to the tiny-but-crucial baryon asymmetry $\eta_B \equiv (n_B - n_{\bar{B}})/n_\gamma = (6.1 \pm 0.2) \times 10^{-10}$ [3,116].[24] Such tracking is typical of scenarios in which $B - L$ is a conserved quantum number and leptogenesis is the forerunner of baryogenesis. However, several models are known in which a small η_B is accompanied by a large η_ν [117,118]. Consequently, it is worth our while to examine the observational constraints on the neutrino asymmetry.

A significant lepton asymmetry in the early Universe, represented by a nonvanishing chemical potential ξ_α, would increase the expansion rate of the Universe, increasing the amplitude of the acoustic peaks observed in the cosmic microwave background anisotropy. A combined analysis of CMB and SN Ia data [119] finds $-0.01 \leq \xi_e \leq 0.22$ and $|\xi_{\mu,\tau}| \leq 2.6$ at 95% C.L. (The ν_e asymmetry is more tightly constrained because it influences the neutron-to-proton ratio at the epoch of big-bang nucleosynthesis, and hence the helium fraction.) If neutrino mixing equilibrates all the chemical potentials before big-bang nucleosynthesis, then the bound for ξ_e applies to all species [120], and $|\xi_{\nu\alpha}| < 0.1$ [121–123], whereupon in the current Universe $n_{\nu_\alpha} \approx 56\,\mathrm{cm}^{-3}$. However, if a majoron field should block neutrino oscillations in the primordial plasma [124–126], then ξ_μ and ξ_τ do not equilibrate with ξ_e. If we take the largest allowed values, $|\xi_{\mu,\tau}| \simeq 3$, then a large lepton asymmetry appears, $n_{\nu_\alpha} - n_{\bar{\nu}_\alpha} \simeq n_{\nu_\alpha} \simeq 1050\,\mathrm{cm}^{-3}$ [127]. The increased neutrino density would reduce the interaction length for annihilation on the favored relic-neutrino species.

B. Neutrinoless Universe

It is conceivable that neutrinos may interact in ways not foreseen in the standard electroweak theory. If, for example, the neutrinos couple to an extremely light boson, relic neutrinos might annihilate at late times, greatly reducing—indeed, likely erasing—the neutrino density expected in the standard cosmology with standard-model interactions [62]. (Such models appear to be generically in conflict with the angular power spectrum of the cosmic microwave background [128].) If no neutrino relics remain in the recent ($z \lesssim 20$) Universe, then no neutrino absorption lines will be observed. To demonstrate that the search for absorption lines has covered the right terrain, it will be extremely helpful to establish the absolute scale of neutrino masses.

[24]The apparent electrical neutrality of the Universe implies a similarly small electron-positron asymmetry.

C. Neutrino clustering

One early inspiration for the study of ultrahigh-energy neutrino absorption was the prospect that massive neutrinos, with masses in the range 30–100 eV, might account for the dark matter in the Universe [20]. Had that been the case, neutrinos might have been absorbed not only on relics at large redshift, but also on relics clustered in galactic halos. For neutrino masses in the range we now consider likely, $m_\nu \lesssim 0.1$ eV, gravitational clustering of neutrinos appears to be insignificant [129]. Moreover, since light neutrinos would cluster—or accrete onto other structures—only at late times, absorption spectroscopy is unlikely to record neutrino density contrasts [17]. The question of detecting neutrino clumps by other techniques remains open.

VI. SUMMATION AND OUTLOOK

Let us assess the prospects for developing cosmic-neutrino absorption spectroscopy as a new window on Nature. First, we require that neutrino observatories establish the existence of cosmic-neutrino fluxes that extend to energies in the Greisen-Zatsepin-Kuzmin regime and beyond. If the requisite neutrino fluxes exist, then the essential task will be to observe absorption lines at energies corresponding to the masses of one or more neutrino species. Making those observations will require detectors with vast effective volumes, or long exposure times, or both. Detecting the relic-neutrino background would, by itself, be an enormously satisfying observational accomplishment. A survey of other techniques that might detect the relics is given in Ref. [127]. Short of direct detection, it may be possible to quantify the influence of primordial anisotropies in the relic neutrinos upon the cosmic microwave background [130,131].

The observation of cosmic-neutrino absorption lines will open the way—at least in principle—to new insights about neutrino properties and the thermal history of the Universe. Our calculations, with their successive inclusion of potentially significant effects, show that how the tale unfolds will depend on factors we cannot foresee. The earlier in redshift the relevant cosmic-neutrino sources appear, the lower the present-day energy of the absorption lines and the denser the column of relics the superhigh-energy neutrinos must traverse. In particular, the appearance of dips at energies much lower that we expect points to early—presumably nonacceleration—sources, that could give us insight into fundamental physics at early times and high-energy scales. On the other hand, integration over a longer range in redshift means more smearing and distortion of the absorption lines.

If the lightest neutrino mass is small, then Fermi smearing due to the thermal motion of the relics sets an effective

lower bound on the neutrino mass, as reflected in the absorption lines. That moves the absorption lines to lower, more accessible, energies, but reduces the power of absorption-line spectroscopy to distinguish the neutrino mass eigenstates. Once the age of the cosmic-neutrino sources is clear, analyzing the thermal smearing may provide at least a rough measurement of the current temperature of the relic neutrinos. In the best (imaginable) circumstance, discriminating the interactions of electron, muon, and tau neutrinos might enable future experiments to determine, or verify, the flavor content of the mass eigenstates.

It appears relatively secure to conclude that future observations of the ν_e/ν_μ ratio at the first absorption dip can decide whether the neutrino mass hierarchy is normal or inverted. Accelerator-based long-baseline neutrino-oscillation experiments should be the first to measure the sign of the ''atmospheric'' mass-squared difference. This is not necessarily a losing proposition for cosmic-neutrino absorption spectroscopy: the more information—neutrino masses, flavor composition, etc.—other experiments provide to neutrino observatories, the more perceptive cosmic-neutrino absorption spectroscopy might become about the thermal history of the Universe.

The experiments we describe in this study will not be done very soon, and their interpretation is likely to require many waves of observation and analysis. Nevertheless, they offer the possibility to establish the existence of another relic from the big bang and, conceivably, they may open a window on periods of the thermal history of the Universe not readily accessible by other means.

ACKNOWLEDGMENTS

Fermilab is operated by Universities Research Association Inc. under Contract No. DE-AC02-76CH03000 with the U.S. Department of Energy. One of us (C. Q.) is grateful for the hospitality of the Kavli Institute for Theoretical Physics during the program, *Neutrinos: Data, Cosmos, and Planck Scale.* This research was supported in part by the National Science Foundation under Grant No. PHY99-07949. G. B. and O. M. acknowledge the stimulating environment of the Aspen Center for Physics. G. B. thanks the Fermilab Theory Group for the support of its summer visitors program. We thank Nicole Bell, Andreas Ringwald, and Tom Weiler for informative discussions, and Yvonne Wong for a helpful remark. Our calculations made extensive use of the Fermilab General-Purpose Computing Farms [134].

[1] S. Weinberg, *Gravitation and Cosmology: Principles and Applications of the General Theory of Relativity* (Wiley, New York, 1972).
[2] G. Steigman, Annu. Rev. Nucl. Part. Sci. **29**, 313 (1979).
[3] Particle Data Group, S. Eidelman *et al.*, Phys. Lett. B **592**, 1 (2004).
[4] E. W. Kolb and M. S. Turner, *The Early Universe* (Perseus/Westview, Boulder, 1993).
[5] E. Harrison, *Cosmology: the Science of the Universe* (Cambridge University Press, Cambridge, England, 2000).
[6] A. Liddle, *An Introduction to Modern Cosmology* (Wiley, New York, 2003).
[7] S. Dodelson, *Modern Cosmology* (Academic, New York, 2003).
[8] C. L. Bennett *et al.*, Astrophys. J. Suppl. Ser. **148**, 1 (2003). A summary table of cosmological parameters is available at http://lambda.gsfc.nasa.gov/product/map/wmap_parameters.cfm.
[9] V. Barger, J. P. Kneller, H. S. Lee, D. Marfatia, and G. Steigman, Phys. Lett. B **566**, 8 (2003).
[10] S. S. Gershtein and Ya. B. Zeldovich, Pis'ma Zh. Eksp. Teor. Fiz. **4**, 174 (1966) [JETP Lett. **4**, 120 (1966)].
[11] R. Cowsik and J. McClelland, Phys. Rev. Lett. **29**, 669 (1972).
[12] G. L. Fogli, E. Lisi, A. Marrone, A. Melchiorri, A. Palazzo, P. Serra, and J. Silk, Phys. Rev. D **70**, 113003 (2004).
[13] Super-Kamiokande Collaboration, Y. Fukuda *et al.*, Phys. Rev. Lett. **81**, 1562 (1998).
[14] SNO Collaboration, Q. R. Ahmad *et al.*, Phys. Rev. Lett. **89**, 011301 (2002).
[15] KamLAND Collaboration, K. Eguchi *et al.*, Phys. Rev. Lett. **90**, 021802 (2003).
[16] G. Duda, G. Gelmini, and S. Nussinov, Phys. Rev. D **64**, 122001 (2001).
[17] A. Ringwald and Y. Y. Y. Wong, J. Cosmol. Astropart. Phys. 12 (2004) 005.
[18] T. J. Weiler, Phys. Rev. Lett. **49**, 234 (1982).
[19] T. J. Weiler, Astrophys. J. **285**, 495 (1984).
[20] E. Roulet, Phys. Rev. D **47**, 5247 (1993).
[21] P. Gondolo, G. Gelmini, and S. Sarkar, Nucl. Phys. **B392**, 111 (1993).
[22] S. Yoshida, H. Y. Dai, C. C. H. Jui, and P. Sommers, Astrophys. J. **479**, 547 (1997).
[23] B. Eberle, A. Ringwald, L. Song, and T. J. Weiler, Phys. Rev. D **70**, 023007 (2004).
[24] T. Han and D. Hooper, New J. Phys. **6**, 150 (2004).
[25] P. J. E. Peebles and B. Ratra, Rev. Mod. Phys. **75**, 559 (2003).
[26] W. L. Freedman and M. S. Turner, Rev. Mod. Phys. **75**, 1433 (2003).
[27] M. Trodden and S. M. Carroll, in *Particle Physics and Cosmology: The Quest for Physics beyond the Standard Model(s) (TASI 2002)*, edited by H. E. Haber and A. E. Nelson (World Scientific, Singapore, 2004), p. 703.
[28] For recent reviews, see the rapporteur talks by Clark McGrew, Yifang Wang, and Paul Langacker at the 2004 International Conference on High Energy

Physics (Beijing), available at http://ichep04.ihep.ac.cn/program.htm.
[29] Mini-BooNE Run Plan, available at http://www-boone.fnal.gov/publicpages/runplan.ps.gz.
[30] LSND Collaboration, C. Athanassopoulos *et al.*, Phys. Rev. Lett. **77**, 3082 (1996).
[31] B. Kayser, in Ref. [3], Sec. 13.
[32] KamLAND Collaboration, T. Araki *et al.*, Phys. Rev. Lett. **94**, 081801 (2005).
[33] E. Kearns, in Proceedings of Neutrino 2004, available at http://neutrino2004.in2p3.fr/slides/tuesday/kearns.pdf.
[34] T. Nakaya, in Proceedings of Neutrino 2004, available at http://neutrino2004.in2p3.fr/slides/tuesday/nakaya.pdf.
[35] CHOOZ Collaboration, M. Apollonio *et al.*, Phys. Lett. B **466**, 415 (1999).
[36] K. Anderson *et al.*, hep-ex/0402041.
[37] Y. Itow *et al.*, in *Proceedings of the 8th ISSP International Symposium on Correlated Electrons, Kashiwa, Japan, 2001* (University of Tokyo, Tokyo, 2001), p. 239; for additional information, see http://neutrino.kek.jp/jhfnu/.
[38] NOvA Collaboration, I. Ambats *et al.*, FERMILAB Proposal No. 0929, available at http://www-nova.fnal.gov/.
[39] O. Mena and S. Parke, Phys. Rev. D **70**, 093011 (2004).
[40] CERN working group on Super Beams, J. J. Gomez-Cadenas *et al.*, hep-ph/0105297.
[41] A. Cervera, A. Donini, M. B. Gavela, J. J. Gomez Cadenas, P. Hernandez, O. Mena, and S. Rigolin, Nucl. Phys. **B579**, 17 (2000); **B593**, 731(E) (2001).
[42] C. Albright *et al.*, hep-ex/0008064.
[43] J. Burguet-Castell, D. Casper, J. J. Gomez-Cadenas, P. Hernandez, and F. Sanchez, Nucl. Phys. **B695**, 217 (2004).
[44] J. Burguet-Castell, M. B. Gavela, J. J. Gomez-Cadenas, P. Hernandez, and O. Mena, Nucl. Phys. **B646**, 301 (2002).
[45] A. Donini, E. Fernandez-Martinez, P. Migliozzi, S. Rigolin, and L. Scotto Lavina, Nucl. Phys. **B710**, 402 (2005).
[46] T. Yanagida, in *Proceedings of the Workshop on the Baryon Number of the Universe and Unified Theories, Tsukuba, Japan, 1979*, edited by O. Sawada and A. Sugamoto, pp. 95–98, available at http://neutrino.kek.jp/seesaw/KEK-79-18-Yanagida.pdf.
[47] M. Gell-Mann, P. Ramond, and R. Slansky, hep-ph/9809459.
[48] R. N. Mohapatra and G. Senjanovic, Phys. Rev. Lett. **44**, 912 (1980).
[49] M. Fukugita and T. Yanagida, Phys. Lett. B **174**, 45 (1986).
[50] S. R. Elliott and P. Vogel, Annu. Rev. Nucl. Part. Sci. **52**, 115 (2002).
[51] J. N. Bahcall, H. Murayama, and C. Pena-Garay, Phys. Rev. D **70**, 033012 (2004).
[52] Y. Farzan, O. L. G. Peres, and A. Y. Smirnov, Nucl. Phys. **B612**, 59 (2001).
[53] Y. Farzan and A. Y. Smirnov, Phys. Lett. B **557**, 224 (2003).
[54] KATRIN, Karlsruhe Tritium Neutrino Experiment, http://www-ik1.fzk.de/tritium/.
[55] A. D. Dolgov, Phys. Rep. **370**, 333 (2002).
[56] S. Hannestad, New J. Phys. **6**, 108 (2004).
[57] P. Crotty, J. Lesgourgues, and S. Pastor, Phys. Rev. D **69**, 123007 (2004).
[58] J. Lesgourgues, S. Pastor, and L. Perotto, Phys. Rev. D **70**, 045016 (2004).
[59] The Two-Degree Field Galaxy Redshift Survey obtained spectra for 245 591 objects, mainly galaxies; see http://www.mso.anu.edu.au/2dFGRS/.
[60] The Sloan Digital Sky Survey is measuring the distances to more than a million galaxies and quasars; see http://www.sdss.org.
[61] U. Seljak *et al.*, astro-ph/0407372 [Phys. Rev. D (to be published)].
[62] J. F. Beacom, N. F. Bell, and S. Dodelson, Phys. Rev. Lett. **93**, 121302 (2004).
[63] H. Päs and T. J. Weiler, Phys. Rev. D **63**, 113015 (2001).
[64] S. M. Bilenky, C. Giunti, J. A. Grifols, and E. Masso, Phys. Rep. **379**, 69 (2003).
[65] R. Gandhi, C. Quigg, M. H. Reno, and I. Sarcevic, Phys. Rev. D **58**, 093009 (1998).
[66] M. H. Reno, Nucl. Phys. B, Proc. Suppl. **143**, 407 (2005).
[67] R. Gandhi, C. Quigg, M. H. Reno, and I. Sarcevic, Astropart. Phys. **5**, 81 (1996).
[68] M. Takeda *et al.*, Phys. Rev. Lett. **81**, 1163 (1998); see also http://www-akeno.icrr.u-tokyo.ac.jp/AGASA/results.html.
[69] High Resolution Fly's Eye Collaboration, R. U. Abbasi *et al.*, Phys. Rev. Lett. **92**, 151101 (2004).
[70] V. Berezinsky, hep-ph/0303091.
[71] K. Greisen, Phys. Rev. Lett. **16**, 748 (1966).
[72] G. T. Zatsepin and V. A. Kuzmin, Pis'ma Zh. Eksp. Teor. Fiz. **4**, 114 (1966) [JETP Lett. **4**, 78 (1966)].
[73] F. W. Stecker, Astrophys. J. **228**, 919 (1979).
[74] F. W. Stecker, J. Phys. G **29**, R47 (2003).
[75] E. Waxman and J. N. Bahcall, Phys. Rev. D **59**, 023002 (1999).
[76] V. S. Berezinsky, in *Proceedings of the International Conference on Neutrino Physics and Neutrino Astrophysics (Neutrino '77)*, edited by M. A. Markov *et al.* (Nauka, Moscow, 1978), Vol. 1, p. 177.
[77] EGRET Collaboration, P. Sreekumar *et al.*, Astrophys. J. **494**, 523 (1998).
[78] The Gamma Ray Large Area Space Telescope, http://www-glast.stanford.edu.
[79] P. Bhattacharjee, C. T. Hill, and D. N. Schramm, Phys. Rev. Lett. **69**, 567 (1992).
[80] D. V. Semikoz and G. Sigl, J. Cosmol. Astropart. Phys. 04 (2004) 003.
[81] V. S. Berezinsky and A. Vilenkin, Phys. Rev. D **62**, 083512 (2000).
[82] O. E. Kalashev, V. A. Kuzmin, D. V. Semikoz, and G. Sigl, Phys. Rev. D **65**, 103003 (2002); **66**, 063004 (2002).
[83] A. W. Strong, I. V. Moskalenko, and O. Reimer, in *Proceedings of the 28th International Cosmic Ray Conference, Tsukuba, Japan, 2003* (Universal Academy Press, Tokyo, 2003), pp. 2687–2690.
[84] C. T. Hill, Nucl. Phys. **B224**, 469 (1983).
[85] R. Aloisio, V. Berezinsky, and M. Kachelriess, Nucl. Phys. B, Proc. Suppl. **136**, 319 (2004).
[86] R. Davis, Rev. Mod. Phys. **75**, 985 (2003).
[87] M. Koshiba, Int. J. Mod. Phys. A **18**, 3109 (2003) [Rev. Mod. Phys. **75**, 1011 (2003)].

[88] The AMANDA Collaboration, J. Ahrens *et al.*, astro-ph/0409423.
[89] The BAIKAL Collaboration, C. Spiering *et al.*, astro-ph/0404096.
[90] I. Kravchenko, astro-ph/0306408.
[91] R. M. Baltrusaitis *et al.*, Phys. Rev. D **31**, 2192 (1985).
[92] W. Y. Lee *et al.*, in *Proceedings of the 26th International Cosmic Ray Conference, Salt Lake City, UT, 1999*, edited by B. L. Dingus *et al.*, AIP Conf. Proc. No. 516 (AIP, New York, 2000), Vol. 2, p. 483. For the High Resolution Fly's Eye, see http://hires.physics.utah.edu.
[93] AGASA Collaboration, N. Hayashida *et al.*, Astropart. Phys. **10**, 303 (1999).
[94] P. W. Gorham, K. M. Liewer, C. J. Naudet, D. P. Saltzberg, and D. R. Williams, astro-ph/0102435.
[95] N. G. Lehtinen, P. W. Gorham, A. R. Jacobson, and R. A. Roussel-Dupre, Phys. Rev. D **69**, 013008 (2004).
[96] IceCube, http://icecube.wisc.edu, is a one-cubic-kilometer international high-energy neutrino observatory being built and installed in the clear deep ice below the South Pole Station.
[97] ANTARES, Astronomy with a Neutrino Telescope and Abyss environmental RESearch, http://antares.in2p3.fr.
[98] P. Piattelli, talk given at Neutrino 2004, Paris: http://neutrino2004.in2p3.fr/slides/friday/piattelli.ppt.
[99] NESTOR, Neutrino Extended Submarine Telescope with Oceanographic Research, http://www.nestor.org.gr.
[100] L. F. Thompson, talk given at Neutrino 2004, Paris: http://neutrino2004.in2p3.fr/slides/friday/lthompson.ppt.
[101] J. F. Beacom, N. F. Bell, D. Hooper, S. Pakvasa, and T. J. Weiler, Phys. Rev. Lett. **90**, 181301 (2003).
[102] ANITA, ANtarctic Impulsive Transient Antenna, http://www.ps.uci.edu/~barwick/anitaprop.pdf.
[103] E. Zas, talk given at Neutrino 2004, Paris: http://neutrino2004.in2p3.fr/slides/friday/zas.ppt.
[104] S. Bottai, talk given at Neutrino 2004, Paris: http://neutrino2004.in2p3.fr/slides/friday/bottai.ppt; see also http://www.euso-mission.org.
[105] D. B. Cline and F. W. Stecker, astro-ph/0003459; see also http://owl.gsfc.nasa.gov.
[106] H. Athar, M. Jezabek, and O. Yasuda, Phys. Rev. D **62**, 103007 (2000).
[107] G. Barenboim and C. Quigg, Phys. Rev. D **67**, 073024 (2003).
[108] G. Gelmini, G. Varieschi, and T. Weiler, Phys. Rev. D **70**, 113005 (2004).
[109] J. F. Beacom, N. F. Bell, D. Hooper, S. Pakvasa, and T. J. Weiler, Phys. Rev. D **68**, 093005 (2003).
[110] J. W. F. Valle, Phys. Lett. **131B**, 87 (1983).
[111] G. B. Gelmini and J. W. F. Valle, Phys. Lett. **142B**, 181 (1984).
[112] Z. Chacko, L. J. Hall, T. Okui, and S. J. Oliver, Phys. Rev. D **70**, 085008 (2004).
[113] C. T. Hill, D. N. Schramm, and T. P. Walker, Phys. Rev. D **36**, 1007 (1987).
[114] C. Spiering, J. Phys. G **29**, 843 (2003) [Nucl. Phys. B, Proc. Suppl. **125**, 1 (2003)].
[115] F. Halzen and D. Hooper, J. Cosmol. Astropart. Phys. 01 (2004) 002.
[116] WMAP Collaboration, D. N. Spergel *et al.*, Astrophys. J. Suppl. Ser. **148**, 175 (2003).
[117] I. Affleck and M. Dine, Nucl. Phys. **B249**, 361 (1985).
[118] J. A. Casas, W. Y. Cheng, and G. Gelmini, Nucl. Phys. **B538**, 297 (1999).
[119] S. H. Hansen, G. Mangano, A. Melchiorri, G. Miele, and O. Pisanti, Phys. Rev. D **65**, 023511 (2002).
[120] C. Lunardini and A. Y. Smirnov, Phys. Rev. D **64**, 073006 (2001).
[121] A. D. Dolgov, S. H. Hansen, S. Pastor, S. T. Petcov, G. G. Raffelt, and D. V. Semikoz, Nucl. Phys. **B632**, 363 (2002).
[122] Y. Y. Y. Wong, Phys. Rev. D **66**, 025015 (2002).
[123] K. N. Abazajian, J. F. Beacom, and N. F. Bell, Phys. Rev. D **66**, 013008 (2002).
[124] K. S. Babu and I. Z. Rothstein, Phys. Lett. B **275**, 112 (1992).
[125] L. Bento and Z. Berezhiani, Phys. Rev. D **64**, 115015 (2001).
[126] A. D. Dolgov and F. Takahashi, Nucl. Phys. **B688**, 189 (2004).
[127] G. Gelmini, talk given at Nobel Symposium 129: Neutrino Physics, Enköping, Sweden, 2004, http://www.physics.kth.se/nobel2004/talks/G_Gelmini-Prospects_of_relic_neutrino_searches.pdf.
[128] S. Hannestad, J. Cosmol. Astropart. Phys. 02 (2005) 011.
[129] S. Singh and C. P. Ma, Phys. Rev. D **67**, 023506 (2003).
[130] W. Hu, D. Scott, N. Sugiyama, and M. J. White, Phys. Rev. D **52**, 5498 (1995).
[131] R. Trotta and A. Melchiorri, astro-ph/0412066.
[132] O. Mena and S. J. Parke, Phys. Rev. D **69**, 117301 (2004).
[133] J. F. Beacom and N. F. Bell, Phys. Rev. D **65**, 113009 (2002).
[134] M. Albert *et al.*, Report No. FERMILAB-TM-2209l, available at http://library.fnal.gov/archive/test-tm/2000/fermilab-tm-2209.pdf.